A Numerical Study of Dual Core Surface Plasmon Resonance-based Photonic Crystal Fiber Biosensors.

by

Anan Adrita

Submitted in partial fulfillment of the requirements

for the degree of Master of Applied Science

at

Dalhousie University
Halifax,Nova Scotia
April 2024

I dedicate this thesis to my family.

Table of Contents

List of Figures

Abstract

Photonic crystals (PCs) are periodic material structures in the optical domain. Felix Bloch developed a theory that describes how electron waves behave in the periodic structure of solids such as semiconductors. The same theory can be applied in an optical domain, and it can explain how photons or light waves behave in periodic crystals. In essence, photonic crystals are artificial materials structured to possess a periodic modulation of refractive index so that the structure influences the propagation and confinement of light within it. Several researchers have demonstrated PCs' exceptional properties in the domain of photonic-crystal-fibers (PCF)-based surface-plasmon-resonance (SPR) biosensors. There is often a tradeoff between sensitivity and confinement loss of these sensors. To reduce this tradeoff, we achieved greater sensitivity while incurring a few losses by creating two distinct sensor designs: unique, susceptible, and easy to fabricate. The analysis of both sensors has been conducted using the finite element method based on COMSOL Multiphysics software. Structural design and theoretical modeling have been done for proposed designs 1 and 2, SPR-based PCF biosensors. The designs have been optimized by varying several parameters, such as the thickness of plasmonic material, air hole diameter, analyte layer thickness, pitch variation, and perfectly matched layer variation. The corresponding confinement losses were also calculated. Mode analysis was performed, and the physics-controlled mesh was used in FEM-based software. Both prototypes have a particular arrangement of air holes within the fiber, resulting in exceptional sensing capabilities. Proposed design 1 is a dual-core PCF with a wide sensing range of refractive index (RI) from 1.21 to 1.40. Maximum amplitude sensitivity of 1096RIU^{-1}, wavelength sensitivity of 7000nm/RIU, and maximum sensor resolution of 5×10^{-5} have been achieved, respectively. A diverse array of biomolecules can be detected using this design. This biosensor was further analyzed to identify three types of cancer cells: basal, Jurkat, and MCF-7. Confinement losses, resonant conditions, and wavelength shifts were examined. The numerical analysis showed that the maximum sensitivity achieved was 878RIU^{-1} for the skin's basal cells. Proposed design 2 is a plasmonic RI sensor for detecting low RI using a sensitive dual core PCF. Maximum amplitude sensitivity of 393RIU^{-1}, wavelength sensitivity of 12000nm/RIU, and resolution of 8.33×10^{-6} have been obtained, respectively. Plasmonic material, silver, was applied externally to the fiber structure to monitor variations in the RI of the surrounding medium.

List of Abbreviations and Symbols Used

PC	Photonic Crystal
SPR	Surface Plasmon Resonance
SPP	Surface Plasmon Polariton
RI	Refractive Index
THz	Terahertz
PMMA	Polymethyl methacrylate
HDPE	High-density polyethylene
EML	Effective material loss
IR	Infrared
TIR	Total Internal Reflection
MTIR	Modified total internal reflection
θ_c	Critical angle
n1	Refractive index of the first medium
n2	Refractive index of the second medium
θ_1	Angle of incidence
θ_2	Angle of refraction
n_{fsm}	Effective fundamental space-filling mode
β	propagation constant
k	Free space wave number
DNA	Deoxyribonucleic acid
ELISA	Enzyme-linked immunosorbent assay
CCD	Charge-coupled device
CMOS	Complementary metal oxide semiconductor

LSPR	Localized surface plasmon resonance
β_{sp}	Propagation constant of a surface plasmon
ε_m	Complex permittivity
ω	Angular frequency
c	Speed of light in vacuum
Neff	Effective refractive index
γ_i	Attenuation coefficient
θ	Angle of incidence
n_p	The refractive index of the prism
Λ	Diffraction grating period
λ	wavelength
m	Diffraction order
FBG	Fiber Bragg grating
FOM	Figure Of Merit
TiN	Titanium Nitride
TiO_2	Titanium dioxide
ITO	Indium Tin Oxide
SiO_2	Silicon dioxide
tg	Gold layer thickness
ta	Analyte layer thickness
PML	Perfectly matched layer
PBG	Photonic band gap
p	pitch
α	confinement loss
Im_{neff}	Imaginary effective refractive index
AS	Amplitude sensitivity

n_{si}	The refractive index of silica
n_{TiO2}	The refractive index of Titanium dioxide

Acknowledgment

I would like to thank my supervisor Professor Michael Cada for giving me this wonderful opportunity to conduct my graduate studies under his supervision. I'm also grateful for his thorough guidance and feedback, inspiration and patience, all through the dissertation work.

Chapter 1) Introduction

1.1) Background

Since their invention, photonic crystal fiber (PCF) sensors have advanced rapidly. In 1968, Bergmann was the first to describe an optical sensor that used fluorescence cooling to detect oxygen. Since then, numerous interdisciplinary studies in chemistry, biology, physics, electronics, and optical sciences have been merged with photonics and optical sensors. Optical sensors combining interdisciplinary research in electro optics, photonics, physics, materials, chemistry, and biology have been realized. The development of optical detecting systems and devices, as well as light sources covering a broad wavelength range from ultraviolet (UV) to infrared (IR), has occurred during the previous few decades.
Interest in fiber-optic sensors for advancing contemporary measurement technologies has grown steadily. Interferometric fiber-optic sensors are highly relevant because of their numerous advantages over conventional sensors—their sensitivity to electromagnetic interference, versatility in responding to different measurements, extreme resolution, high precision, and compact size. Some interferometric fiber-optic sensors have been successfully commercialized and commonly used for composite material health monitoring, sizeable civil engineering systems (e.g., bridges and dams), rockets, aircraft, etc., creating intelligent materials and structures [1].

A biosensor is a self-contained integrated device capable of providing specific quantitative or semi-quantitative analytical information using a biological recognition element in direct spatial contact with a transducer element. In other words, it can also be considered a sensor that integrates a biological element with a physiochemical transducer to produce an electronic signal proportional to a single analyte, which is then conveyed to a detector. A biosensor is a device that uses specific biochemical reactions to detect chemical compounds in biological samples. Figure 1.1 shows the schematic representation of a biosensor.

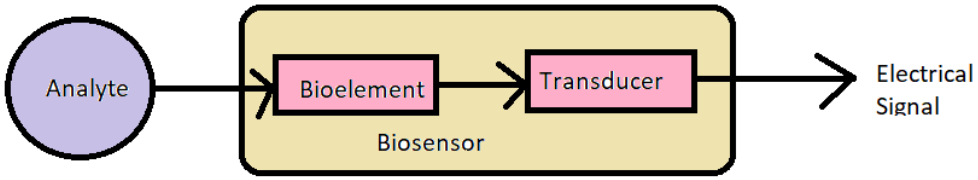

Figure 1.1- Schematic representation of a biosensor.

Optical biosensors have unique benefits compared to conventional profiling methods for monitoring and analyzing molecular interactions. It represents the most common type of biosensor, which has drawn the researcher's attention for the past couple of decades due to its wide range of applications in various established fields such as drug discovery, healthcare, food quality control, biotechnology industry, and environmental safety monitoring. [2] Biosensors are analytical tools used to detect specific analytes such as Cholesterol, Urea, Penicillin, Ethanol, etc., having biomolecules such as nucleic acids, proteins, and carbohydrates as crucial elements for detecting these analytes [3].

We are polluting the environment in terms of air, water, and food. For example, we are spraying pesticides on crops to grow more and more food. The remnants of these pesticides exist in the food. These can lead to many diseases like cancer, diarrhea, bacterial infection, contaminated food, growth inhibition, and diabetes. We are subjected to various diseases. The advantages of optical biosensors are that they are small, flexible, fast, and safe because no electrical device interacts with the body. They have good biocompatibility. According to the market overview, biosensors have a vast potential and requirements. Figure 1.2 shows the biosensor US market

size by technology from 2020 to 2030.

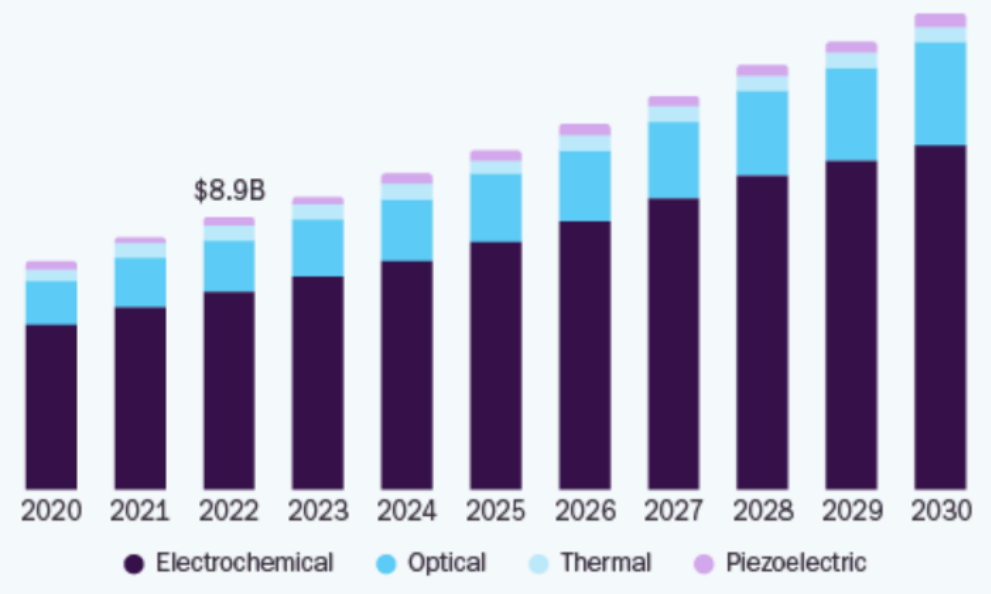

Figure 1.2- Biosensors US market size from 2020 to 2023

1.2) Problem Statement

In 1993, R.C. Jorgenson suggested using optical fiber as the first sensor based on surface plasmon resonance (SPR). This involved coating the fiber core with a gold film by selectively removing a portion of the fiber cladding, which allowed for observing the plasmonic response[4]. In an SPR sensor, it is necessary to satisfy the phase matching condition, where the core-guided fundamental mode, surface plasmon polaritons (SPP) mode, and propagation loss peak coincide at a specific wavelength. During this stage, the resonance peak will shift to identify the unknown analyte to the particular wavelength. Recently, there has been significant interest in developing high-performance photonic crystal fiber sensors based on surface plasmon resonance (PCF-SPR). These sensors offer advantages such as single-mode transmission without cutoff, high sensitivity, and the ability to measure several parameters.

A conventional type of sensor is based on an internal sensing mechanism where the metal film is coated internally [5]. One drawback of this method is that emptying and refilling the fiber is time-consuming. The layer that is coated internally is highly fragile, which adds complexity to fabrication and structure. A. Rifat *et al*. examined a SPR sensor that utilized a photonic PCF with analyte channels that were selectively filled and a core that had a deposition of graphene-silver. The sensor demonstrated a refractive index sensitivity of 3,000 nm/RIU, the highest value

observed [6]. S. Jiao *et al.* studied a dual-core PCF-based SPR sensor consisting of a segmented silver film coated on the microfluidic channel with an average sensitivity of 5,100 nm/RIU [7]. A PCF-SPR sensor filled with gold nanoshells was presented, which achieved a wavelength sensitivity of 4111.4 nm/RIU with a sensor resolution of 2.45 × 10−5 RIU in the RI range from 1.330 to 1.380 [8]. Hasan *et al.* introduced a circular lattice PCF-SPR sensor composed of two air hole rings, with the first ring having two missing air holes. The sensor demonstrated a maximum sensitivity of 2200 nm/RIU within the refractive index (RI) range of 1.330 to 1.360 [9]. These sensors offer narrow sensing ranges and weak sensitivity. The problems reported in these SPR-based sensors are complicated design, fabrication difficulty, increased confinement loss, and uneconomical cost.

1.3) Research Objective and Motivation

PCF, or photonic-crystal fiber, is a unique optical fiber with exceptional waveguiding capabilities. It can contain light more effectively than any of the existing conventional optical fibers. Numerous PCF applications, including fiber optic interchanges, fiber lasers, non-linear devices, high control transmission, various gas sensors, data transmission in the THz regime, etc., have been discovered by researchers. PCFs are typically made of a micro-structured arrangement with air holes distributed along the fiber's length and undoped silica as the backdrop material. The area surrounding the core is called cladding, while the inner part is known as the core. Our research aimed to create and examine the impact of innovative and distinct designs of PCF biosensors utilizing SPR technology. The research has the following precise objectives:

- Obtain phase matching conditions of both proposed design 1 and proposed design 2.
- To quantify the sensitivity of amplitude (AS) and wavelength (WS) to changes in refractive index across a range of wavelengths for both designs.
- Plasmonic materials are employed externally to the photonic crystal fiber (PCF) structure to enhance detection accuracy and improve overall performance.
- Investigation of the effects on performance and graphical outcomes resulting from minor parameter variations. Simulation of many characteristics by altering the thickness of different fiber layers such as Gold, Titanium dioxide (TiO2), analyte, etc.

1.4) Thesis Framework

This thesis report includes seven distinct chapters chapters. A brief synopsis of the upcoming six chapters is provided in this section.

Chapter 2 introduces Photonic Crystal fibers. A cross-sectional view of PCF is illustrated along with various possible design variations. A comparison is drawn between conventional fibers and PCF. A thorough discussion on 1D,2D,3D, and artificial PCs is done. Finally, PCFs are classified based on various parameters like structure, guiding mechanism, material, and bandgap properties.

Chapter 3 introduces SPR phenomena. It gives an overview of SPR and discusses its advantages. Chapter 3 also demonstrates localized SPR phenomenon and SPR sensorgrams

Chapter 4 introduces SPR based PCF biosensors. It widely classifies the sensor based on sensing mechanisms and various plasmonic materials.

Chapter 5 demonstrates proposed design 1 which is dual core PCF with a wide sensing range. It illustrates the structural and theoretical modeling of the biosensor, its guiding properties, and its dispersion characteristics. Several design parameters are optimized such as air hole diameter, gold layer thickness, analyte layer thickness, etc to achieve the best performance and sensitivity of the proposed biosensor. Chapter 6 is about proposed design 2 which is a plasmonic RI sensor for detecting low RI using very sensitive dual core. Numerical design, modeling, and phase-matching conditions are achieved in this chapter. Wavelength and amplitude sensitivities, resolution, and sensing range are calculated by varying various design parameters. Several graphs are plotted corresponding to these variations.

In Chapter 7 applications of PCF and fabrication techniques are discussed. Proposed design 1 is implemented to detect various cancer cells. The results are shown by plotting confinement loss vs wavelength graphs for breast, skin, and blood cancer.

Chapter 8 discusses the socio-economic impact, and future work related to this paper and includes a comprehensive summary of this paper.

Chapter 2) Photonic Crystal Fiber

2.1) Introduction

The refractive index of the core of a standard optical fiber is higher than that of the cladding. To make the core material's refractive index greater than the silica cladding, the core is doped with a high refractive index substance. Fluorine is typically utilized to lower the refractive index, and germanium is used to raise the refractive index of the core. Photonic crystal fiber is a dielectric medium with minimal loss, created by arranging small air holes in a periodic pattern that spans the entire length of the fiber. Photon confinement in the core of a photonic crystal fiber (PCF) results in superior waveguiding capabilities compared to conventional optical fiber. A solid silica core in PCF enables the core to guide the optical signal effectively. A regular arrangement of air holes in the outer layer encompasses the central part. Due to the lower effective cladding index than the core refractive index, the light signal can be guided along the silica core through total internal reflection. The air holes contribute to the low-index cladding.

The core is typically created by either enlarging an air hole in its location or eliminating an air hole from the center of the structure. Photonic crystal fibers (PCFs) offer several design parameters that can be adjusted to achieve desired characteristics, such as the core radius, number of rings, air hole diameter, and pitch (distance between air holes). Application of guiding properties can be gained by modulating these parameters as the guiding properties of optical fibers depend on the refractive index, and the refractive index of PCFs depends on those design freedoms [10]. PCF SPR sensors have high sensitivity and lower resonance peaks than fiber-based sensors [11]. Figure 2.1 illustrates the cross-sectional view of PCF.

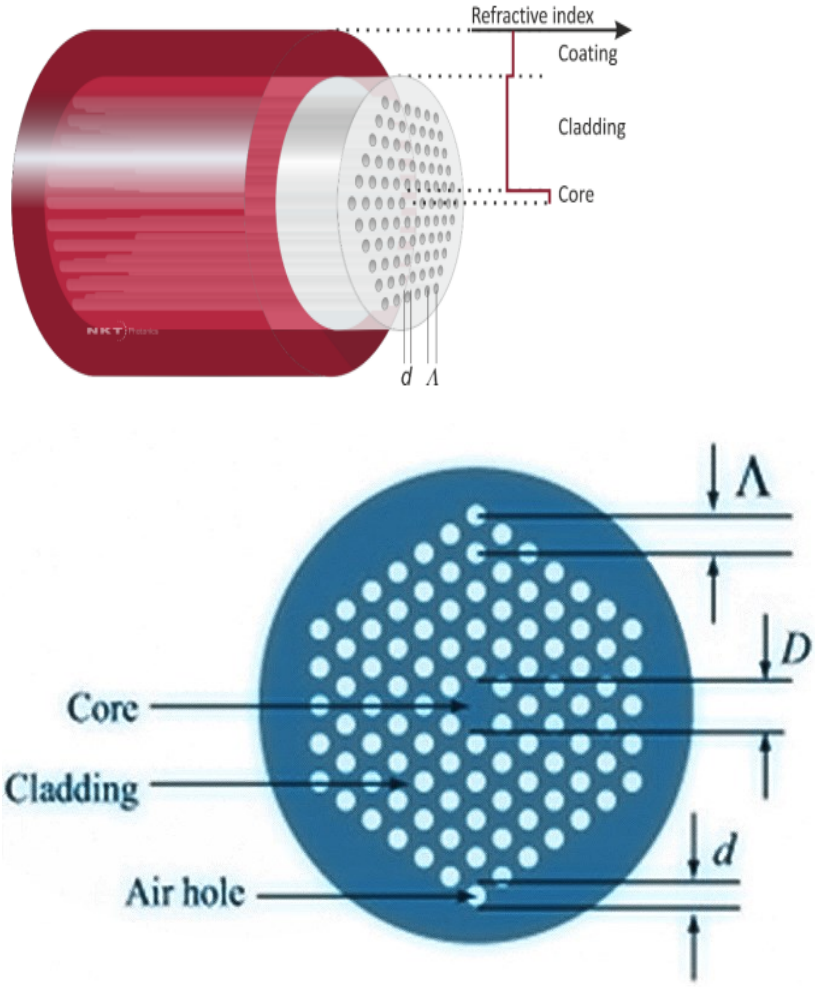

Figure 2.1- Cross Sectional View of Photonic Crystal Fiber[12].

2.2) PCF Design Variations

The background material used in PCF is not limited to silica alone.[13] Different crystal fibers such as Teflon [14], PMMA [15], TOPAS [16], [17], and HDPE [18]are commonly used. TOPAS is regarded as the most suitable material for waveguide propagation due to its extraordinary water barrier properties [17] and excellent biosensing characteristics [19]. For porous fiber, birefringence is one of the crucial parameters that is effective for polarization-maintaining sensing applications [20]. The structure of a PCF's core and cladding regions carries a significant role in fiber performance. The honeycomb cladding structure was initially tested by

J. Lægsgaard et al. [21][22]. After that, many designs have increased because of improved design flexibility and fabrication facilities. Some efficiently implemented designs are square [23], hexagonal [24], octagonal [25], spiral [26], circular [27], and hybrid[28]. In contrast to other fibers, substantial attention has been given to the porous core fibers due to their capability of maintaining low EML (effective material loss), high birefringence, and higher power into the core region simultaneously [29]. Thus, we can see that many PCF designs are possible, and good results can be obtained using PCs. PCF is a compact and lightweight structure that allows miniaturization of the sensors, which makes them more feasible for remote sensing [30].

2.3) Conventional fiber vs PCF

Light can propagate through the air core in photonic crystal fiber. The surrounding medium is a photonic bandgap. Light cannot penetrate the photonic bandgap, so it automatically goes through the fiber. This contrasts with the traditional optical fiber, where light propagates through total internal reflection. In photonic crystal fiber, the arrangement of the surrounding cladding is such that light cannot propagate through it. The fiber might get burned when transferring a large amount of power. One of the ways to overcome this is to create a photonic crystal fiber with a hollow core. The cladding can be made with various layers of dielectric. Intense carbon dioxide laser light at a 10-micron wavelength range can be guided through the core. It can be used for strong light transmission as light will not be dispersed. Figure 2.3 shows the differences between conventional optical fiber and PCF.

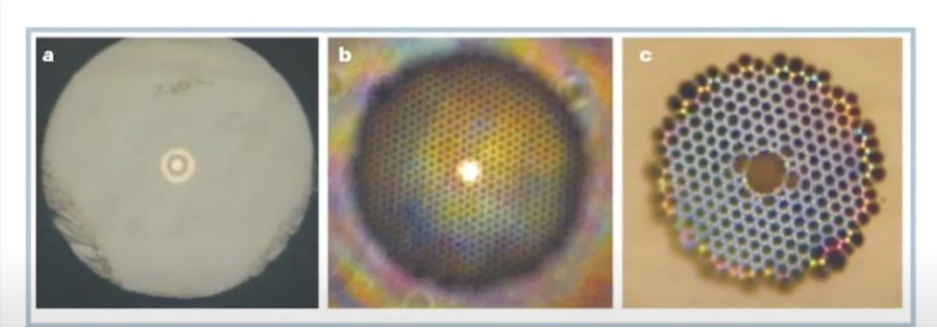

Figure 2.3- (a) Conventional fiber with a core diameter of 9 microns (b) Dielectric-core PCF Core diameter of 5 microns (c) Air-core PCF Core diameter of 9 microns [31].

2.4) 1D, 2D and 3D photonic crystals-

1D PC is an array of thin films. It was not possible to get bandgap in all different directions with 1D PCs. If we have various angles of incidence, we will have electromagnetic waves propagating through the material. It is challenging to get an omnidirectional photon band gap. The immediate alternative is to think of a two-dimensional arrangement of materials. In silicon substrate, air holes can be arranged so that photonic bandgap can be achieved in all possible directions for all angles of incidence. This is one of the features of the omnidirectional reflector. The wave will be reflected at any particular angle for this type of structure. In the case of photonic crystals with one dimension, it is challenging to get high reflection at all points, but it is possible with 2D geometry, and it is one of the critical successes in this area. This is among the most popular geometry studies by various research groups worldwide. Yablonovich et al. proposed photonic crystal fibers in three dimensions. He originally proposed the idea of a hexagonal lattice in three dimensions. It turns out that holes need to be created not just in vertical directions but in all three directions, which requires lots of analysis and unique insights. This type of structure had bandgaps in all different directions. In a way, this could be said to be the birth of photonic crystals. The only problem was that this structure was to be drilled in alumina, and the holes were significant compared to their tools. It operates in mm frequencies. This type of structure would not work in the visible domain because the sizes are much smaller; visible frequencies have high energy, so smaller dimensions are necessary. After this, there was a surge in research interest among various groups to compete and create artificial photonic crystals. In 1996, Krauss et al. and others showed the first 2D photonic crystals that were operating near IF. In the development of photonic crystals, the challenge has been the accessibility of nanofabrication techniques. This was one of the critical requirements in this area.

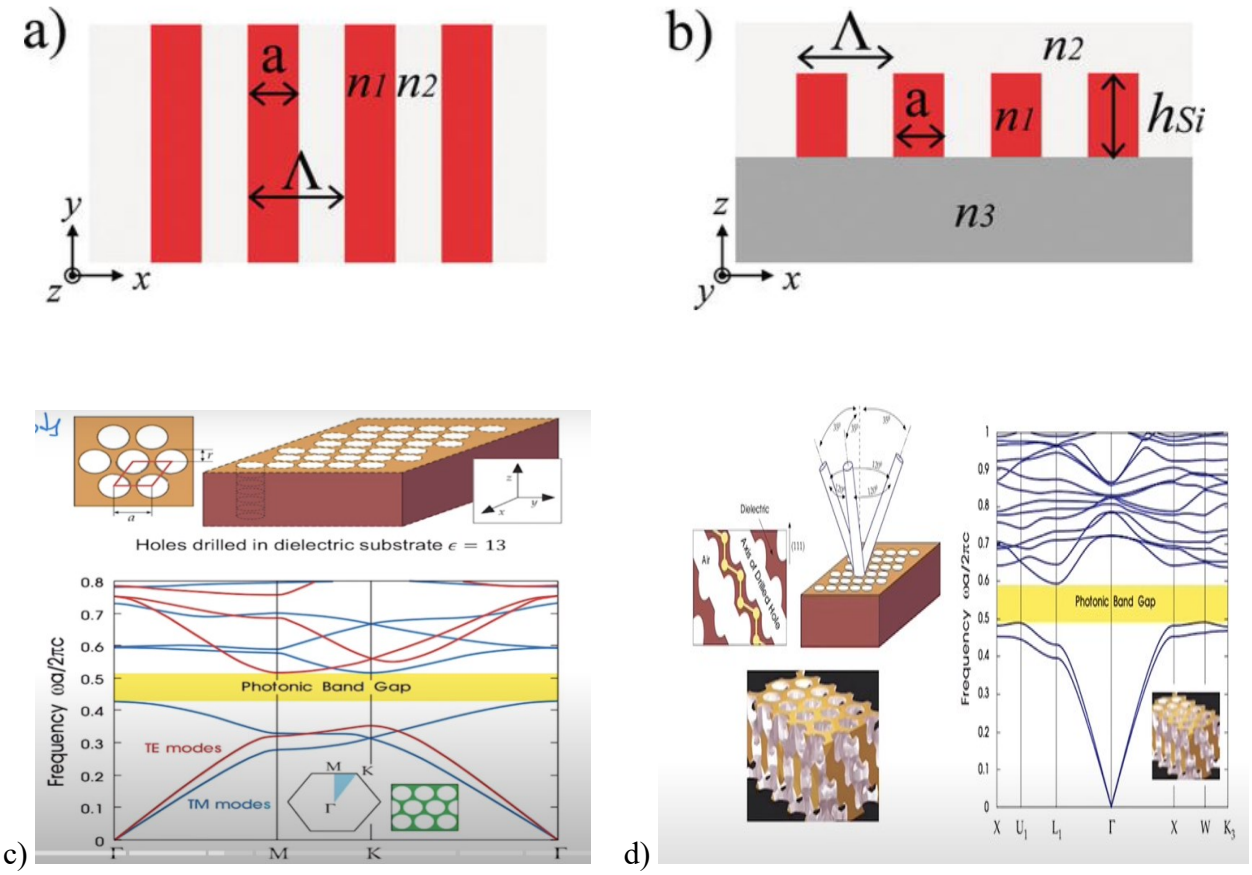

c) d)

Figure 2.4- a) Top View and (b) cross-sectional view of 1D Photonic crystals[32], (c) 2D photonic crystal fiber, (d) 3D photonic Crystal [31].

2.5) Artificial photonic crystal-

Artificial photonic crystals operate near the visible IR range. It is a woodpile structure where silicon strips are arranged. Every alternating layer has the perpendicular orientation of the strips, and the arrangement of this unit strip leads to the creation of photonic crystals. It was implemented in 1998. A lot of different fabrication techniques were explored to create 3D photonic crystals.

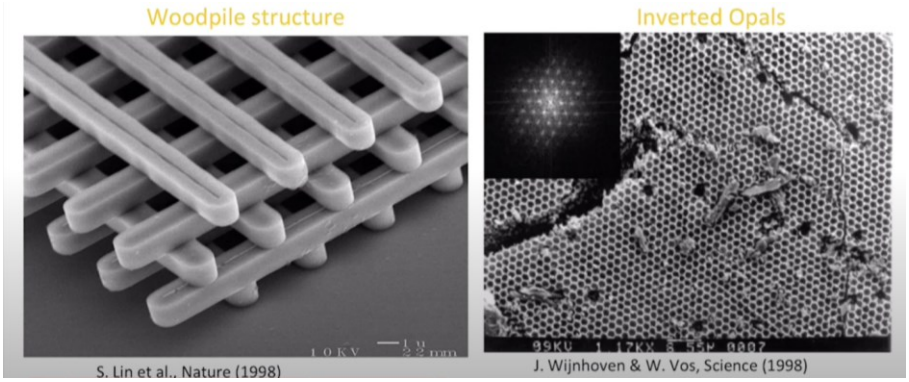

Figure 2.5- Examples of the structure of Artificial Photonic Crystals [31].

The woodpile structure is manufactured by taking a piece of silicon dioxide and then etching it. The structure is filled with silicon again. Lines of silicon dioxide are made where gaps are filled with silicon. This is called polysilicon. After the silicon trench filling process is repeated perpendicularly until the desired number of layers is obtained. Eventually, after the structure is finished, it is dipped into hydrofluoric acid to etch away silicon dioxide. Fabrication is quite intensive in photonic crystals.

2.6) Classification of PCF

Photonic crystal fibers (PCFs) are a distinct type of optical fibers that utilize a regular arrangement of materials to provide distinctive optical characteristics. They are categorized according to several attributes, such as their composition, guiding mechanism, and practical uses. Below are several typical categorizations of photonic crystal fibers-

2.6.1) Based on Structure

Solid-core PCFs consist of a core composed of solid material, such as silica or another type of glass, comparable to conventional optical fibers. The defining characteristic of solid-core PCFs is their cladding structure, which includes a regular pattern of air holes. This distinctive architecture enables light control by utilizing total internal reflection and photonic bandgap effects. The average refractive index in the cladding is less than the core.

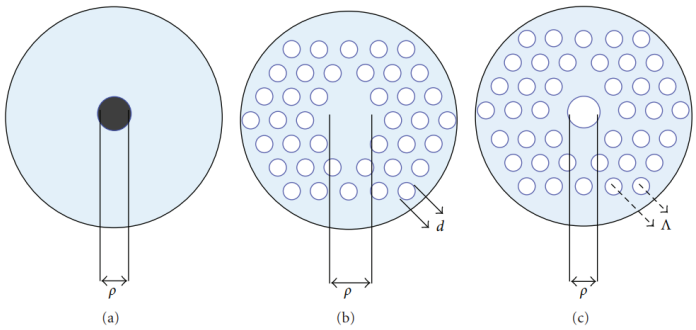

Figure 2.6.1a- Drawing of (a)single-mode fiber, (b)solid core PCF, (c) hollow-core PCF. In the figure, blue represents silica, grey represents doped silica, and white represents air[33].

Solid core PCF

Solid-core PCFs utilize total internal reflection at the core interface and cladding interface to guide light, similar to conventional fibers.

- Effects of Photonic Bandgap: A periodic arrangement in the cladding generates a photonic bandgap, which can selectively permit or obstruct specific wavelengths of light, hence facilitating light guiding.
- Supercontinuum Generation: Solid-core photonic crystal fibers (PCFs) are commonly used to generate supercontinuum, producing a wide range of light frequencies through nonlinear phenomena.
- Nonlinear Optical Processes: The solid-core structure improves nonlinear effects, rendering these fibers appropriate for frequency conversion and parametric amplification applications.
- High-Power Applications: These devices' distinctive configuration enables them to manage laser sources with high power effectively, rendering them valuable in scenarios that demand strong interactions between light and matter.

Benefits:

- Nonlinear Properties: Solid-core Photonic Crystal Fibers (PCFs) can demonstrate superior nonlinearities to conventional fibers, offering prospects for effective nonlinear processes.

- Customized Dispersion: Customizing the dispersion qualities enables applications that demand precise dispersion characteristics.
- Fabrication Complexity:

Manufacturing solid-core photonic crystal fibers with accurate topologies can be intricate and may necessitate sophisticated fabrication processes.

Optical losses in solid-core PCFs can be more significant depending on the design, particularly at longer wavelengths.

Polarization Properties: A solid-core structure can impact the polarization characteristics of guided light, rendering solid-core photonic crystal fibers (PCFs) appropriate for applications that need polarization sensitivity.

Microstructured photonic crystal fiber (PCF) is an optical fiber designed with a regular pattern of air holes or voids along its length. The presence of these air holes results in the formation of a photonic bandgap structure, which imparts distinctive and adjustable optical characteristics absent in conventional optical fibers.

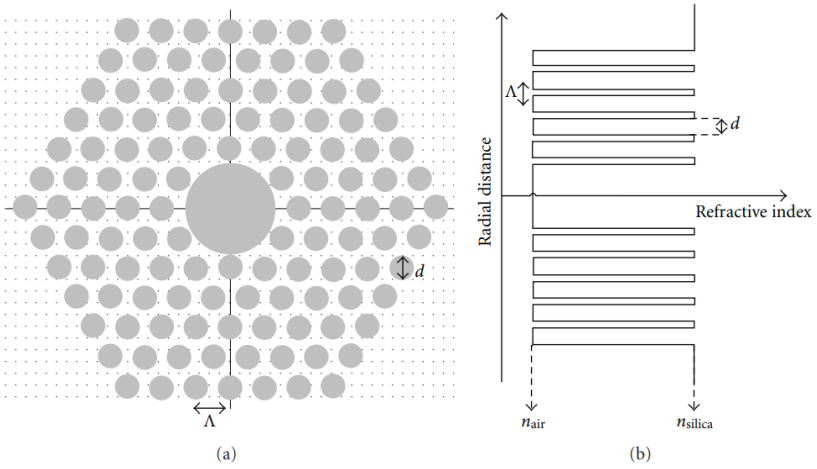

Figure2.6.1b- (a)Illustration of hollow core PCF cross-section and (b)respective refractive index profile [33]

The following are essential characteristics and uses of micro-structured photonic crystal fibers:

A photonic bandgap structure is formed by the periodic arrangement of air holes in the fiber, creating a range of wavelengths in which the propagation of light is forbidden. The photonic

crystal fiber (PCF) bandgap can be customized to specific wavelengths through the PCF's design, enabling accurate manipulation of the fiber's optical characteristics.

- Guiding Mechanism: Unlike traditional fibers, PCFs employ a mix of modified total internal reflection and photonic bandgap phenomena to guide light. This distinctive guiding method allows precise control over dispersion, confinement, and other optical properties.
- Customizable Dispersion: A notable benefit of microstructured PCFs is the capacity to manipulate dispersion characteristics. This is essential for applications like supercontinuum generation, where a wide range of light is required.
- Microstructured fibers can demonstrate amplified nonlinear effects due to their specific design. These properties make them well-suited for several applications, including nonlinear optics, wavelength conversion, and the production of new frequencies via processes such as four-wave mixing.

Single-Mode Operation: Photonic Crystal Fibers (PCFs) can be engineered to facilitate single-mode operation, guaranteeing the propagation of only one spatial mode through the fiber. This is crucial for applications where precise control of the mode is essential.
Supercontinuum Generation: The distinctive characteristics of microstructured Photonic Crystal Fibers (PCFs) make them well-suited for supercontinuum generation. This process generates a wide range of light wavelengths through highly intense nonlinear interactions. These applications encompass spectroscopy, microscopy, and telecommunications.

2.6.2) Based on the guiding mechanism

Total internal reflection (TIR)

TIR happens when light through a medium hits another medium's boundary at an angle larger than the critical angle. The critical angle (θc) is the specific angle of incidence at which light undergoes total internal reflection, resulting in the light being ultimately reflected into the original medium instead of refracted. The critical angle can be determined by applying Snell's Law, which establishes a relationship between the angles of incidence and refraction and the refractive indices of the two media under consideration.

Snell's Law is given by $n1Sin\theta_1 = n2Sin\theta_2$ where n1 is the refractive index of the first medium and n2 is the refractive index of the second medium. θ_1 is the angle of incidence, and θ_2 is the angle of refraction. When light is incident at an angle greater than the critical angle(θ_c), the angle of refraction becomes 90 degrees. Therefore $n1Sin\theta_c = n2Sin90$, and $n1Sin\theta_c = n2$. We can determine the critical angle by $\theta_c = sin^{-1}(\frac{n2}{n1})$. If the angle of incidence is greater than the critical angle, TIR occurs, and all the light is reflected in the first medium.

Photonic bandgap guiding mechanism in PCF

In a PCF, the cladding comprises a regularly spaced arrangement of air holes. The regularity of this pattern forms a lattice structure known as a photonic crystal. The configuration of these apertures and the distance separating them create a bandgap within the structure of the photonic crystal.

Within the bandgap, specific wavelengths of light are prohibited from propagating through the structure. This phenomenon bears resemblance to the functioning of electronic bandgaps in semiconductors. However, instead of manipulating electrons, it regulates the transmission of photons. The PCF's core is intentionally positioned outside the bandgap, enabling it to confine light of wavelengths that align with the bandgap within the core. The confinement occurs due to the lattice structure of the photonic crystal, which hinders the propagation of specific wavelengths through the cladding.

Hence, the photonic bandgap guiding mechanism guarantees that the core of the PCF effectively guides light, even when total internal reflection, which is conventionally the primary guiding mechanism, is not dominating.

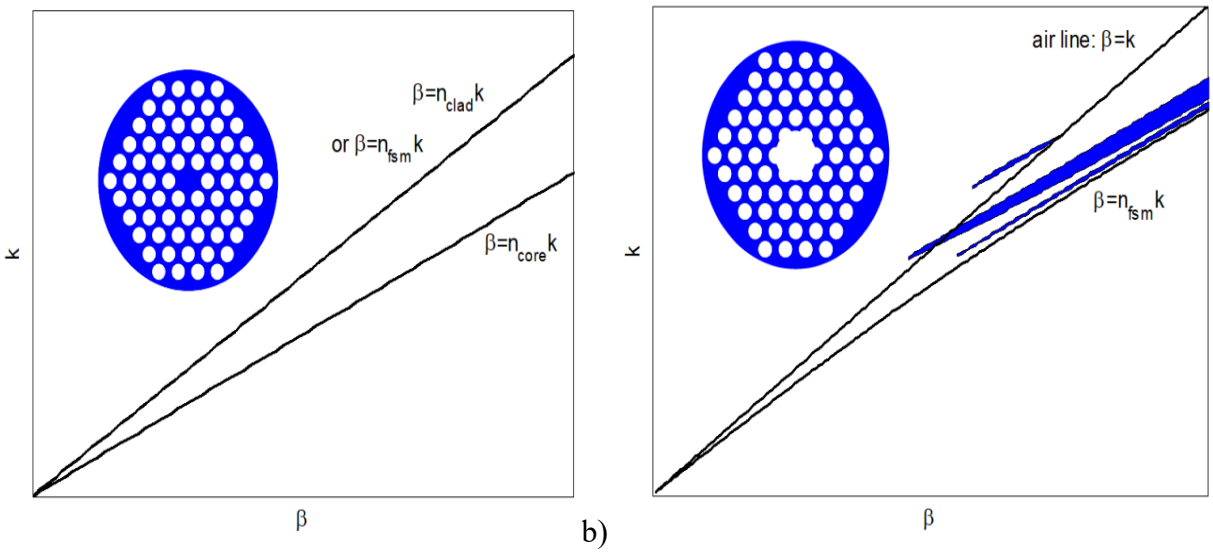

Figure 2.6.2-a)Dispersion curve for index guiding mechanism in conventional optical fibers and solid core PCFs. b) Dispersion curve for PBG-guiding in hollow core PCFs.[34]

Figure 2.6.2 shows the dispersion curve for the index-guiding mechanism in conventional optical fibers and solid core PCFs. The nfsm value is within the refractive index range of air and silica. It can be effectively manipulated by adjusting the holey structure's lattice geometry and air-filling ratio, allowing for either a high-index or low-index contrast. The index-guiding concept is demonstrated in the β-k plot, where β represents the propagation constant and k represents the free space wavenumber, as seen in Figure 2.6.2. In a media that is both homogeneous and isotropic, the point at which total internal reflection (TIR) occurs for light coming from a medium with a higher refractive index is defined by the radiation line β = nk, where n is the refractive index. The critical angle is attained on the radiation line. Light can freely travel above the radiation line, while below the radiation line, the light becomes evanescent. The refractive indices in the core and cladding of standard optical fibers are represented as ncore and nclad, respectively. In index-guiding PCFs, the radiation line β of the holey cladding is given by the equation β = nfsm×k. The diagram depicts a standard solid core PCF with air holes organized in a triangle lattice and implanted in silica. In both conventional optical fibers and index-guiding PCFs, the radiation line of the core is positioned below the radiation line of the cladding. This is because the core area has a higher refractive index. Hence, the optical confinement within the core region of an optical fiber, whether a standard optical fiber or an index-guiding photonic PCF, is limited to the area bounded by the cladding and core radiation lines. The index-guiding

mechanism in index-guiding PCFs is sometimes called the modified total internal reflection (MTIR) guiding mechanism because of its similarities to the guiding mechanism found in traditional optical fibers.

The hollow core is a 'defect' in the photonic crystal structure. The radiation lines of the core and the cladding are denoted as $\beta = k$ and $\beta = nfsmk$, respectively. As the refractive index of the hollow core is lower than nfsm, the core's radiation line lies above the cladding's radiation line.

2.6.3) Based on the core:

Circular Core PCFs: Photonic Crystal Fibres are characterized by a circular core form.

Non-Circular Core PCFs: PCFs that have core forms that are not circular, such as elliptical or hexagonal cores.

2.6.4) Based on usage

Single-mode photonic PCFs are specifically engineered to facilitate the transmission of only one mode of light. They are commonly employed in applications where meticulous manipulation of the light's spatial and temporal characteristics is necessary.

Multimode PCFs are specifically engineered to facilitate the transmission of many modes of light. They are used in situations where a greater light-carrying capacity is needed.

2.6.5) Based on materials:

Silica-based PCFs consist of a core and cladding composed of silica or comparable materials.

PCFs with Alternative Materials: Photonic crystal fibers are fabricated using materials other than silica, such as soft glass, polymer, or other photonic crystal materials.

2.6.6) Based on unique characteristics:

Polarization-maintaining PCFs are designed to preserve light polarization over extended distances, rendering them valuable in applications needing polarization sensitivity.

High Nonlinearity PCFs are specifically engineered to amplify nonlinear optical phenomena, which is crucial in various applications such as supercontinuum generation.

2.6.7) Based on their bandgap properties:

1D, 2D, and 3D PCFs: These terms indicate the dimensionality of the photonic bandgap structure. One-dimensional (1D) photonic crystals exhibit periodicity in one direction, two-

dimensional (2D) photonic crystals exhibit periodicity in two directions, and three-dimensional (3D) photonic crystals exhibit periodicity in three directions.

Chapter 3) Surface Plasmon Resonance

3.1) Introduction

Surface Plasmon Resonance (SPR) is the interaction between light and a metal surface near a dielectric media, such as air or a liquid. These interactions result in the emergence of collective oscillations of electrons on the surface of the metal, which are referred to as surface plasmons. The resonance situation arises when the energy of the incident light aligns with the energy necessary to stimulate these surface plasmons.

SPR is a phenomenon that occurs when polarized light hits a metal film at the interface of media with different refractive indices. It causes collective oscillations of free electrons in the metal. Metals have lots of free electrons. Free electrons resonate along the longitudinal direction when external energy hits the metal. These are called surface plasmons. However, at a specific condition, the frequency of incident light and the frequency of the free electrons are the same. A surface-plasmon wave is generated at this condition, propagating along the metal die electric interface, as shown in Figure 3.1. Until now, several works have been reported that can be categorized as internal and external sensing approaches. When the metal layer is placed outside the fiber, it is called the external sensing approach. There are two types of internal sensing approaches. One is metal layer based. The external sensing approach can be categorized as a D-type structure, a rectangular or flat fiber-based structure, a slotted fiber-based structure, or a conventional external sensing approach.

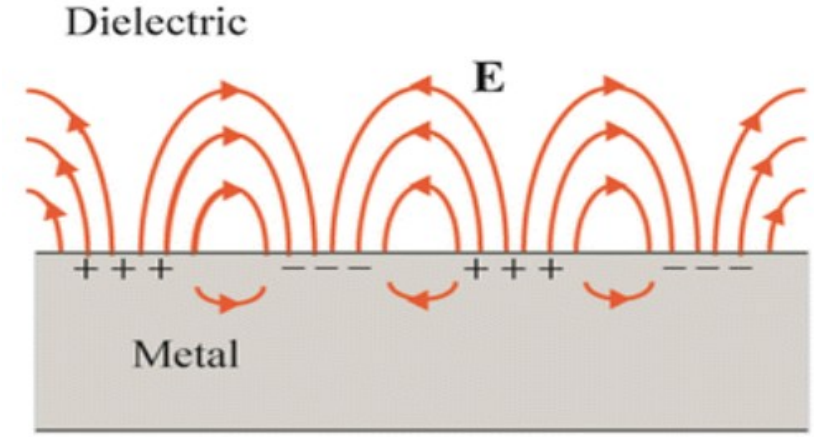

Figure3.1- Surface plasmon wave propagation[35].

3.2) Components of SPR

Below is a comprehensive explanation of the fundamental components of SPR:

- Metal Surface: Surface Plasmon Resonance (SPR) is usually detected on thin metal films, such as gold or silver, placed on a glass substrate. Surface plasmons can propagate on the metal film.
- Incident light refers to the light intentionally focused onto a metal surface at a specified angle, called the angle of incidence. The wavelength of the incident light is a crucial determinant of the resonance state.
- The resonance condition occurs when the incidence angle and the incident light's wavelength meet specific criteria, allowing the energy from the incident photons to be transferred to the collective oscillations of electrons on the metal surface, resulting in the excitation of surface plasmons. Consequently, there is a reduction in the magnitude of the reflected light.
- The sensitivity of the resonance condition to changes in the refractive index of the medium near the metal surface is high. A shift in the resonance angle occurs when molecules attach to or dissociate from the metal surface, leading to any alteration in this index.
- Binding event detection: Surface Plasmon Resonance (SPR) is frequently employed to investigate molecular interactions dynamically. When biomolecules, such as proteins, DNA, or tiny molecules, adhere to the metal surface, the refractive index undergoes a modification, displacing the resonance angle. The shift can be seen and examined to obtain data regarding the rate and strength of the binding interactions.

SPR has been extensively utilized in various disciplines, including biochemistry, molecular biology, and pharmaceutical research. The capacity to offer label-free, instantaneous observation of molecular interactions makes it a powerful instrument for investigating binding kinetics, ascertaining affinities between biomolecules, and conducting screenings for medication candidates. Moreover, SPR technology fabricates biosensors for medical diagnostics and environmental monitoring.

3.3) Advantages of SPR

Real-time monitoring -

The primary advantage of surface plasmon resonance (SPR) in monitoring biomolecular binding interactions, such as protein-protein interactions, is the ability to view the real-time processes of molecule associations and dissociation directly. The instrument's computer software generates a sensorgram, a graphical representation of the SPR signal over time, displaying the association and dissociation curves. While techniques like ELISA and co-immunoprecipitation determine the presence or absence of binding, SPR provides more comprehensive insights into the intricacies of the binding process. This information provides insights into the binding kinetics, including the rates at which molecules bind and unbind in dynamic flow circumstances. It also includes affinity data, crucial for a more comprehensive understanding of the investigated process.

Detection without the use of labels - An outstanding feature that distinguishes SPR from other techniques like ELISA and MST is its label-free nature, as it operates based on optical principles. This technique is more precise as it eliminates the possibility of the labels interfering with the ligand's and analyte's inherent activity, such as antibodies. Additionally, it reduces expenses by eliminating the need for costly fluorescent and radioactive labels and additional reagents necessary for labeled detection.

Limited sample sizes - The sample needed is minimal in a surface plasmon resonance experiment. Thus, a few samples would suffice, mainly if the protein purification process already yields a limited product. Similarly, a reduced amount of time is required to obtain a purified sample for analysis.

Reusable sensor chips - Unlike the microwells used in ELISA, the sensor chip utilized in an SPR experiment has the advantage of being reusable. This strategy is distinct from others because it saves money and minimizes waste. During an SPR experiment, a regeneration buffer can be employed to disrupt the association between the ligand and analyte, allowing for the reuse of the sensors.

The utilization of intricate samples is crucial to purify the sample in most biological investigations to provide precise results and analysis, but this is not the case with SPR analysis.

SPR is an optical technique where the light channel remains separate from the sample without intersecting it. Hence, SPR analysis enables the utilization of uncomplicated and intricate samples, such as serum, blood, plasma, and cell lysate.

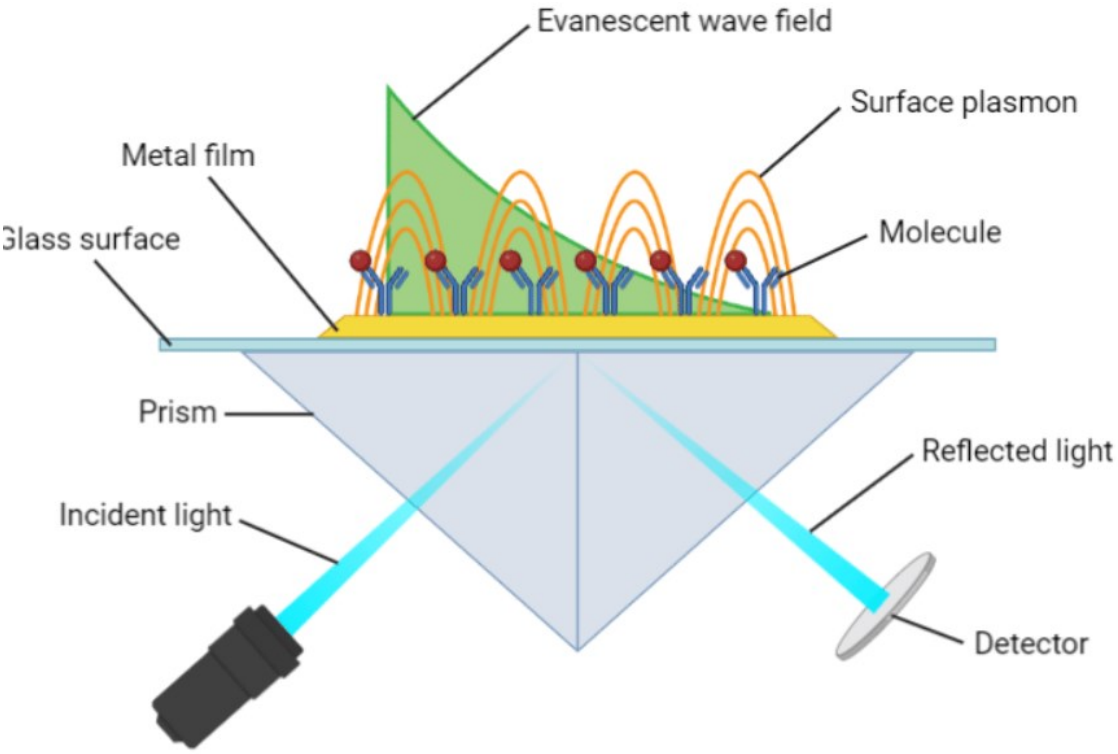

Figure 3.3- Surface plasmon resonance on a metal film in the Kretschmann configuration [36]

Using a surface plasmon resonance instrument requires fewer washing and incubation steps than performing an immunoassay like ELISA, reducing labor and resulting in a shorter experimental time. Consequently, the duration of an SPR run is decreased significantly, with an SPR experiment often taking minutes to a few hours, in contrast to the hours or days required for an ELISA.

3.4) An Overview of SPR

SPR is a promising label-free technique. It is an optical method based on surface plasmon resonance and evanescent waves, which provides kinetic resolution of label-free binding

reactions. SPR spectroscopy biosensors are popular because of their simple instrumentation and high sensitivity. They are also in great demand because they can provide label-free real-time detection of various biomolecular interactions. SPR is used in research for various biological applications, including drug discovery, clinical diagnostics, and security applications.

SPR is a surface-sensitive spectroscopic method that measures the change in the refractive index of a medium directly in contact with the sensor surface, for example, gold.

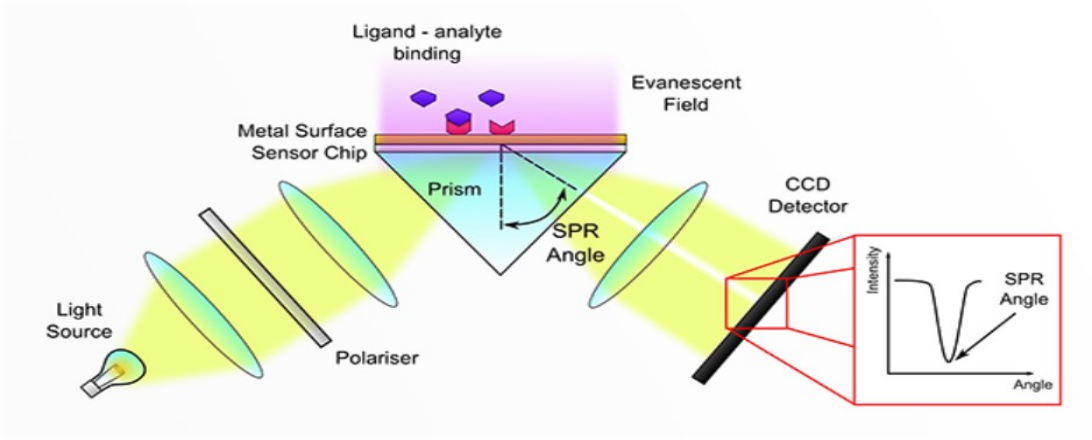

Figure 3.4a illustrates a conventional Kretschmann Configuration, which employs a CCD/CMOS array to capture a broad spectrum of reflected light across various angles. This structure is highly durable, as it only requires a minimal number of components to be moved. Consequently, it may be constructed in a space-saving manner. The extensive array of concurrent measurements also offers substantial versatility in experimental design. However, a drawback is that the angular range that may be measured is typically fixed and challenging for users to modify. Although the range, typically exceeding 10 degrees, is sufficient for most protocols, it can provide challenges when working with less frequently used experimental configurations [37].

As shown in Figure 3.4a, there is a prism, a light source, and antibody immobilization on the gold surface. We can inject the target proteins to be studied through the flow cell. So, a medium in contact with the surface is commonly an aqueous sample containing the analyte protein. Surface plasmons are electromagnetic waves that can be excited at specific metal interfaces.

Gold and silver are mainly used for this purpose. The surface plasmons are electromagnetic waves propagating parallel to the metal or dielectric surface. The plasmons are created from that interface when the light energy from the polarized incident photon is coupled in the oscillation mode of free electron density, which is present in the metal field. These plasmons are generated from gold surfaces at the boundary of the metal and external medium, usually air. These are very sensitive to any changes in the boundary, like the absorption of biomolecules into the metal. In SPR, a light beam impinges at the interface between metal and media at a defined resonance angle. This angle depends upon the refractive index near the gold surface. The refractive index increases when metal binds to the gold surface, and the SPR curve shifts to higher angles. So, these changes in the angle of refraction of light caused by the binding of the probe to the immobilized proteins are measured to characterize biomolecular interactions in real time.

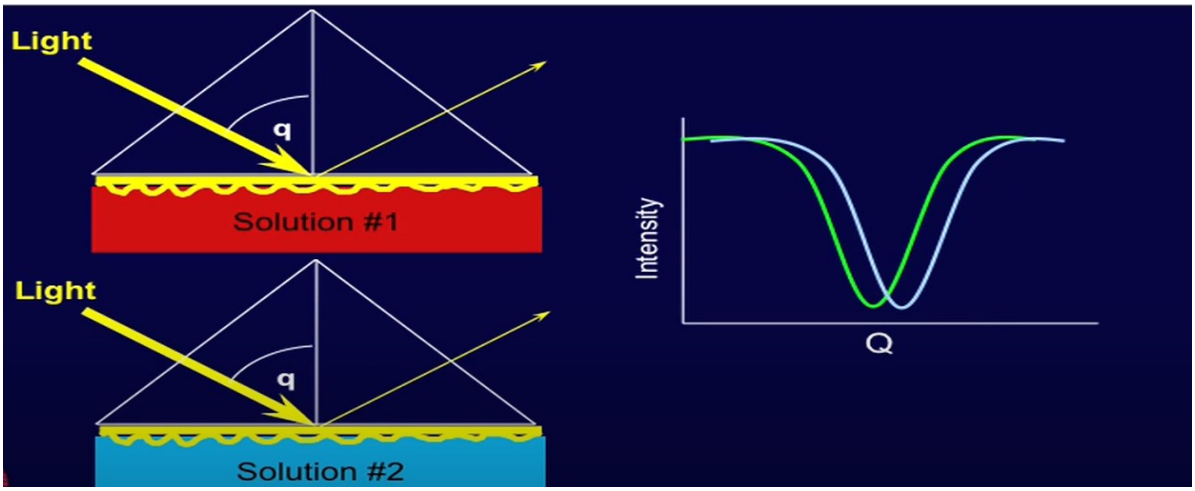

Figure 3.4b)- Diagram showing that SPR angle depends on the refractive index on the surface [38].

SPR angle is related to the number of biomolecules binding to the core surface. The real-time label-free detection of binding events can be detected by measuring changes in SPR reflectivity. These changes in n are continuously monitored to obtain the kinetic data in real time, making it a remarkable label-free detection technique.

3.5) Localized SPR

LSPRs, or localized surface plasmon resonances, refer to the collective oscillations of electron charge in metallic nanoparticles stimulated by light. They have a greater amplitude in the near-field at the resonance wavelength. The field is highly concentrated at the nanoparticle and rapidly diminishes as it moves away from the nanoparticle or the interface with the dielectric. However, the resonance often enhances the scattering of the field in the far-field region by the molecule. The amplification of light intensity is an essential characteristic of localized surface plasmon resonances (LSPRs), and localization guarantees a remarkably high spatial resolution for LSPRs, limited solely by the size of nanoparticles. Due to increased field amplitude, LSPRs often improve effects that depend on the amplitude, such as the magneto-optical effect [39]. Figure 3.5 shows LSPR on the surface of a nanoparticle.

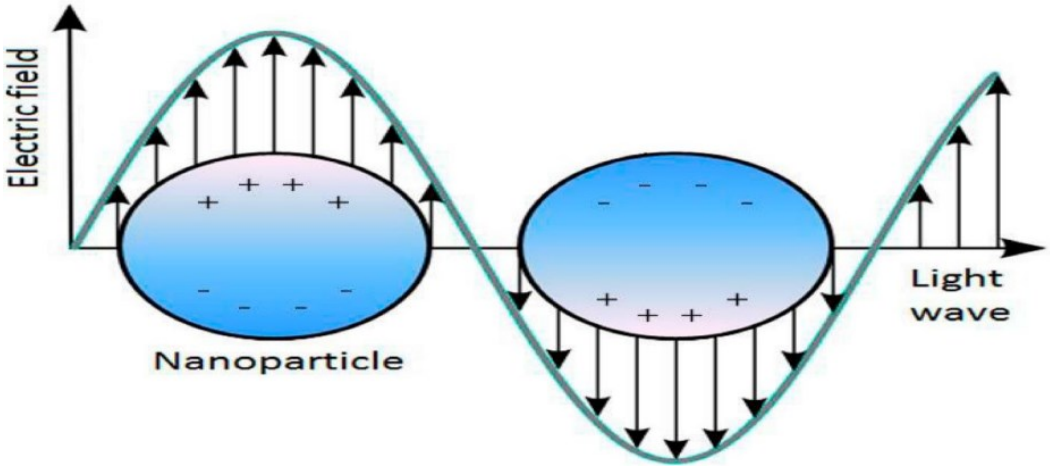

Figure 3.5- Localized Surface Plasmon on the surface of a nanoparticle [40].

3.6) SPR sensorgrams

The sensorgram describes the changes in the SPR signal versus time as molecules bind and dissociate from the sensor surface; the resulting change in resonance signal creates a sensorgram.

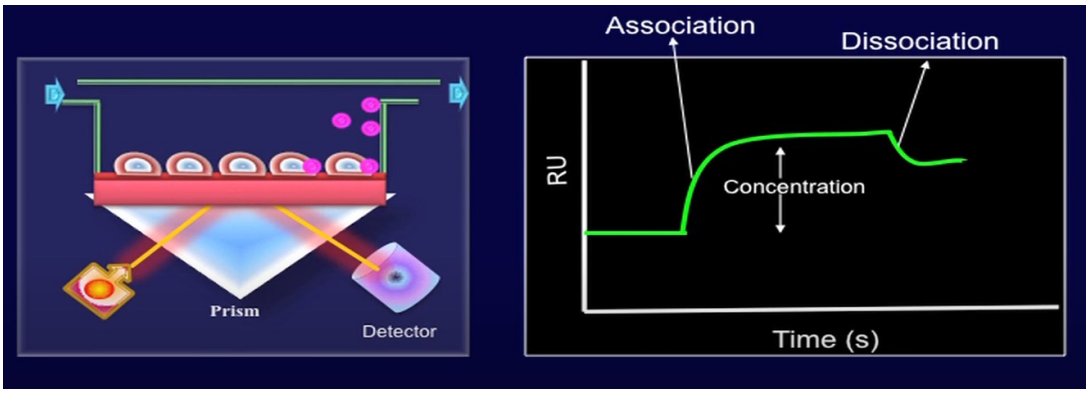

Figure 3.6- Illustration of SPR sensorgram [38].

Figure 3.6 shows a prism, light source, gold-coated chip, and ligand immobilized on the chip surface. The running buffer is initially injected into the immobilized surface, which generates the baseline. The baseline is straight until the analyte is injected into the medium. As the analyte interacts with the surface, an association phase can be observed from which an association rate can be derived. As shown in Figure 3.6, some analyte molecules bind to the chip surface. When the association achieves saturation level, it reaches a state known as a stochastic steady state. Injection of running buffer at this point helps in analyte disassociation from which the dissociation rate can be derived. These curve shapes and amplitude of binding can be used to determine the kinetics of interaction and concentration analysis. The on rate and off rate can provide information on the binding rate. Various analytes can be compared simultaneously by looking at the SPR sensorgrams. The SPR assay means tracking the SPR angles to measure the binding events.

SPR sensors employ the evanescent field of a specific mode of electromagnetic field that travels along a metal/dielectric boundary - known as the surface plasmon - to detect alterations in the refractive index of the dielectric material at the boundary. The propagation constant βsp of a surface plasmon propagating along a flat boundary between a metal with a complex permittivity $\varepsilon m=\varepsilon' m+i\varepsilon'' m$ and a dielectric with a refractive index n can be mathematically represented as

$$\beta_{sp} = \frac{\omega}{c}\sqrt{\frac{n^2\varepsilon_m}{n^2+\varepsilon_m}} = \frac{\omega}{c}(n_{ef}+i\gamma_i),$$

Here, ω represents the angular frequency, and c represents the speed of light in a vacuum. The complex propagation constant can be represented by the effective index (nef) and the attenuation

coefficient (γi) of the surface plasmon [41]. The real and imaginary parts of the propagation constant can be expressed using these parameters.

The primary techniques for optically exciting surface plasmons are attenuated total reflection (prism coupling), diffraction on a metallic grating (grating coupling), and evanescent wave coupling between dielectric and plasmonic waveguides (waveguide coupling). The attenuated total reflection method uses a coupling prism connected to a thin metal film. When light is incident on the interface between the prism and the metal film, it undergoes attenuated total reflection, creating an evanescent wave. This evanescent wave couples with the surface plasmon if the phase-matching requirement is met.

$$\Delta_{ef}^{(prism)} = n_p \sin(\theta) - n_{ef} = 0,$$

The variables are np, which represents the refractive index of the prism; θ, which represents the angle of incidence; and nef, which represents the effective index of the surface plasmon. The excitation of surface plasmons through diffraction coupling necessitates the alignment of the momentum component of the diffracted light wave parallel to the interface and the propagation constant of the surface plasmon.

$$\Delta_{ef}^{(grating)} = n\sin(\theta) + \frac{\lambda m}{\Lambda} - n_{ef} = 0,$$

Where Λ is the diffraction grating period, λ is the wavelength, and m is the diffraction order.

Alterations in the optical properties of the medium adjacent to the immobilized layer will result in modifications to the attributes of the surface Plasmon wave. More precisely, these modifications can be quantified as alterations in wavelength, intensity, phase, or angle of incidence. SPR techniques are prevalent in modern biosensor research due to their ability to detect and analyze interactions between unlabeled substances in real time, making them highly effective for surface-sensitive measurements.

Despite its simplicity and advantages, SPR is not the most sensitive technology. One surface plasmon resonance (SPR) variant involves a resonant mirror configuration that employs a

sequence of polarizing filters to obstruct internally reflected light. At a specific resonance angle, the light is redirected through a spacer layer with a low refractive index into a guide with a higher refractive index, resulting in the signal peak being shown against a black background. Despite these advances, one of the primary limitations of SPR-based biosensors is that anything that alters the refractive index at the sensing surface will interfere with the analysis, including nonhomogeneous (complex) sample matrices and nonspecific binding interactions [42].

Chapter 4) SPR-Based PCF Biosensor

4.1) Introduction

Nowadays, sensors are an essential part of our daily lives. Especially after COVID-19, we have realized the importance of sensors in detecting viruses. If a device responds to a change in the surrounding medium, then we call this device a sensor. Different sensors are available, such as Electrochemical, piezoelectric, and optical. Conventional ELISA and PCR-based sensors require two days to respond because they require several sequential processes to give a specific response.

On the other hand, electrochemical or resistive sensors take a few minutes to respond. Optical sensors can provide an instantaneous response. High sensitivity, fast response, and broad detection range are some advantages of optical sensors. Optical sensors have many applications, such as bioimaging, glucose monitoring, disease detection, telemedicine, medical diagnostics, etc. From 2016 to 2022, the market for photonic sensors has grown very fast. Several types of optical sensors are available, such as Fiber Bragg grating (FBG), modal interferometer, micro-ring resonator, and surface plasmon resonance. Among them, the prism-based plasmonic sensor has shown a highly sensitive response. It has several commercial uses.

Some disadvantages of this type of sensor are that they are complex and bulky systems, they have limited analysis throughput and limited remote sensing applications, and they require oblique light incidence to excite the plasmons. The solution to this problem is a photonic crystal fiber based SPR sensing technique. PCF-based SPR sensor combines photonic crystal fiber-based technology and plasmonic science. PCF is a periodic array of micro-sized air holes. Compared to conventional optical fiber, photonic crystal fiber contains a periodic array of air holes. PCF has been invented in 1996 by Professor Phillip Russel. Light can be trapped in a particular area with the help of PCF.

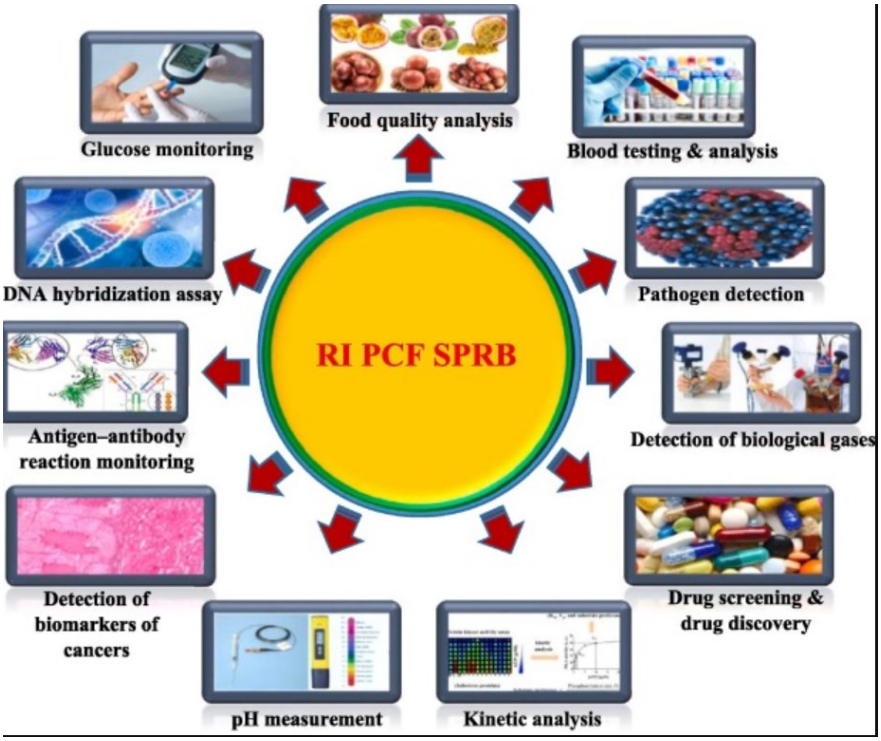

Figure 4.1- Some applications of refractive index SPR based PCF biosensors [43].

4.1.1) Internal Sensing-based Sensor

The internal sensing type sensor was invented to overcome the obstacles of the prism based sensors. Internal sensing is the conventional way of sensing where the air holes are coated with metal films while the analytes are packed within the hole [44]. The practical execution of the first type is intricate due to the challenges of applying metal coatings to the internal fiber holes and filling them with analytes. The challenges emerge due to the minuscule dimensions of the apertures. In addition, it is impossible to keep the holes at a consistent thickness during fabrication. Furthermore, the process of measuring, emptying, and refilling the fiber is necessary, but it is also time-consuming. In addition, the repeated process of filling and emptying can reduce the sensor's sensing capabilities.

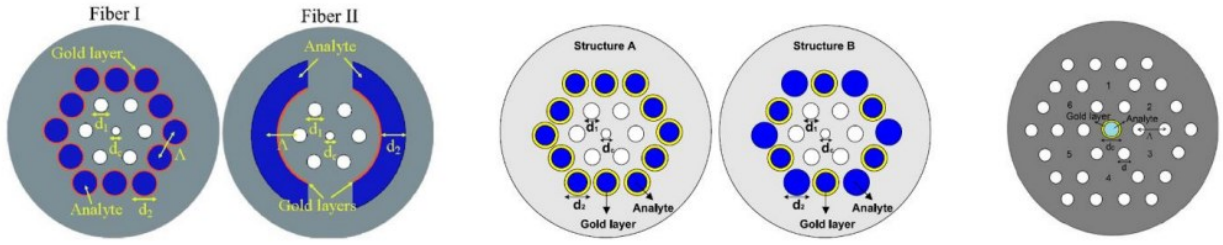

Figure 4.1.1- Internal sensing based sensors [44].

4.1.2) D-shaped Sensors

The use of D-shaped or exposed-core PCFs can help to overcome the disadvantages of prism-based sensors and internal sensing-based sensors [45]. In D-shaped PCFs, the metal and analyte are directly deposited on the exposed surface, as depicted in Figure 4.1.2. This simplifies the process of sensor construction and analyte manipulation. Nevertheless, the flat section of the D-shaped photonic crystal fibers requires polishing, which presents challenges in the manufacturing process. However, in practical application, this sort of sensor requires the selective removal of specific surface portions, introducing additional intricacy in the manufacturing process and resulting in higher sensor costs.

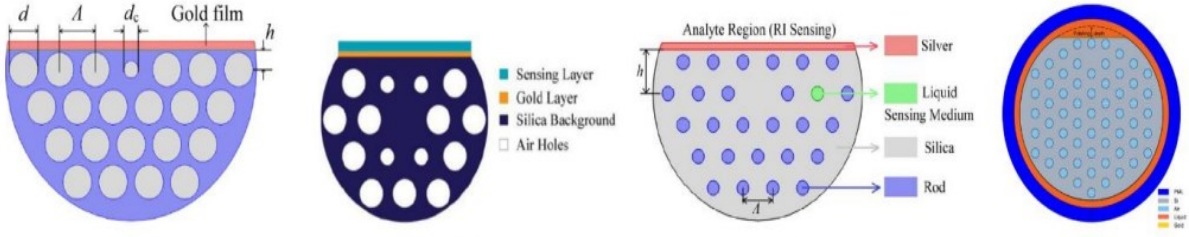

Figure 4.1.2- Various types of D-shaped sensors [46].

4.1.3) External Sensing-based Sensor

Due to the limitations of internal sensing and D-shaped PCF, external sensing has become the preferred method for analyte detection due to its excellent sensing characteristics and the benefit

of the fabrication process [47]. The system offers facilities such as sensor cleaning and reutilization. Unlike internal sensing, where the metal coating is put inside the air holes, the metal coating in external sensing is positioned outside the fiber (as illustrated in Figure 4.1.5-a). This positioning eliminates the need for any pre-steps before sampling. The sensor easily attaches to the analyte solution, and in a short time, it demonstrates the desired sensor performance.

4.1.4) Plasmonic Material Silver based Sensor.

The choice of plasmonic material significantly impacts the sensor's performance. Silver exhibits a distinct resonance peak, resulting in a favorable Figure of Merit (FOM). While silver is very conductive, it is prone to oxidation over time in aquatic environments. This phenomenon diminishes the precision of sensing and impedes the sensor's performance. Due to this chemical instability of silver (Ag) and other limitations, it shows an inaccurate sensing performance [48].

4.1.5) Bimetallic Silver-graphene-based Sensor

Silver oxidizes in a hydrous surrounding, causing a fall in sensing accuracy. An attempt to put a lean coating of graphene has been made to control the oxidization problem, which increases the manufacturing cost and the fabrication difficulties due to additional layers [49].

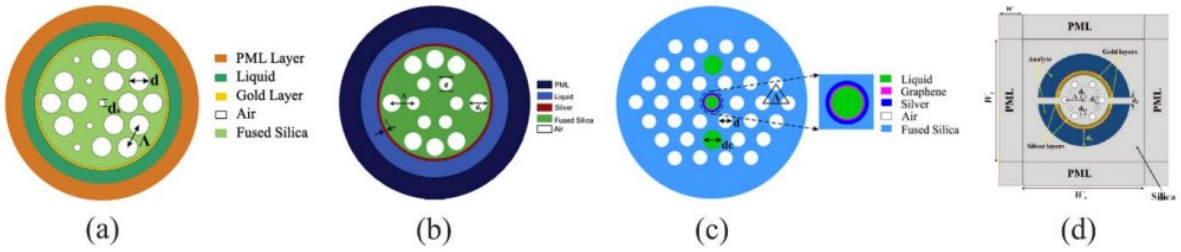

Figure 4.1.5- a) External sensing based sensor, b) Silver-based sensor, c) Silver-Graphene based sensor, d) Silver-Gold based sensor [49]

4.1.6) Bimetallic Silver-gold-based Sensor

This type of SPR-PCF biosensor has two metalized microfluidic slots of gold and silver as plasmonic material. This unique design was proposed by Akowuah et al. in 2012. Gold is positioned at the top of the silver to prevent oxidation and other chemicals. The structure (Figure 6.1.5d) has a more straightforward fabrication process due to large microfluidic slots [50].

4.1.7) Bimetallic Silver-TiN-based Sensor

Traditional bimetallic designs typically incorporate a Gold-Silver coating, with gold as a protective layer. However, gold is hindered by its larger resonance curves, which restrict detection precision. The proposed bimetallic structure can be constructed using silver and TiN, as depicted in Figure 4.4-a. The operational channel is coated with a layer of silver on its surface. An additional layer of TiN was utilized to protect the silver layer from oxidation and to maintain chemical stability [51].

4.1.8) Plasmonic Material Gold-based Sensor

Silver exhibits chemically unstable behavior, although it has sharp resonant peaks. Recently, gold has gained popularity for its chemical stability and capacity to alter the resonance frequency by a significant amount, leading to accurate detection of the analyte. Extensive research has been conducted on biosensors based on gold. A sensor utilizing Gold as the plasmonic material is displayed in Figure 4.1.10 (b).

4.1.9) Bimetallic Gold-TiO2-based Sensor

Gold is utilized as a thin layer to cover the channel in this particular form of sensor. Furthermore, applying a TiO2 coating enhances the surface plasmonic excitation by facilitating the adherence of gold. The increase in the excitation of surface plasmonic leads to an augmentation of the evanescent field. Additionally, it exhibits a greater refractive index (RI) than fiber. It effectively facilitates the coupling between the leaky core guided mode and the plasmonic mode when positioned on the glass surface. Consequently, this layer enhances the ability to detect and perceive stimuli.

4.1.10) ITO-based sensor

The plasmonic resonance of Indium Tin Oxide (ITO) can be adjusted by modifying the intrinsic properties of the materials. Essentially, the plasmonic behavior can be manipulated by adjusting the quantity of oxygen concentration and metal atoms. Furthermore, ITO is a more economical option compared to gold and silver. Figure 4.1.10 showcases a sensor that employs ITO as the plasmonic material.

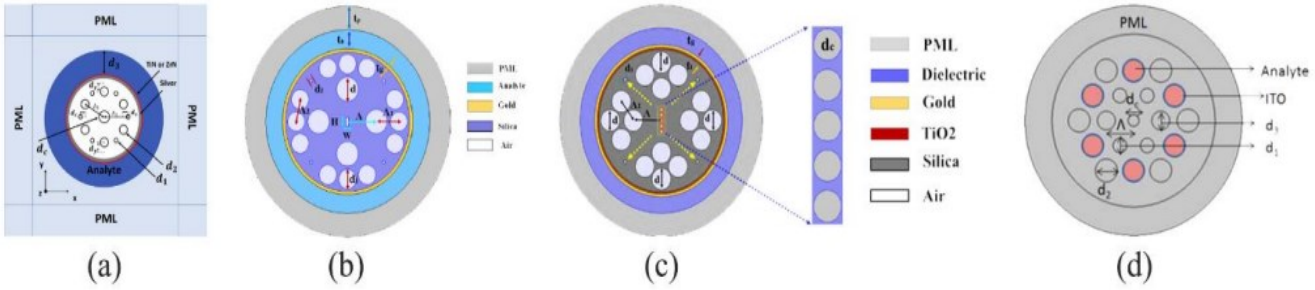

Figure- 4.1.10(a) Silver-TiN based sensor, (b)Gold based sensor, (c) Gold-TiO2 based sensor, (d) ITO-based sensor [52]

Chapter 5) Proposed design 1- Dual core PCF with wide sensing range.

5.1) Introduction

This paper proposes a photonic crystal fiber-based biosensor with a wide sensing range. The numerical analysis of the sensor is done by using finite element method (FEM). Gold (Au) has been used as plasmonic material, resulting in an improved sensing range, operated in the optical to near-infrared (IR) region (0.42-1.0) μm. In addition, the sensor attains a maximum amplitude sensitivity of $1096 RIU^{-1}$, the wavelength sensitivity of 7000nm/RIU, and resolution of 1.43×10^{-5}.

Resonance (SPR) is an optical phenomenon that occurs when free electrons collectively oscillate at the interface between a dielectric and a metal. Resonance occurs when the wavelength of the surface electrons aligns with the wavelength of the incoming photons. The maximal loss for a particular analyte is achieved at the resonant frequency. Even the slightest alterations in the refractive index (RI) result in a shift in the peak, allowing for the detection of an unidentified analyte by the shift in the loss peak and its corresponding wavelength.

SPR sensors are now being extensively used for different sensing applications such as bio-chemical, bio-organic sample detection, medical diagnostic, and medical testing [53]. SPR sensors have been designed based on Kretschmann and Reather's exploiting attenuated total reflection (ATR) mechanism, also called prism-based SPR sensors [54]. Nevertheless, they need plenty of supplementary (mechanical and optical) elements. These sensors are characterized by their large size, high cost, and lack of compatibility for remote sensing. Standard miniaturized sensors based on optical fiber have been proposed to address these constraints. They have effectively surpassed the constraints. Their characteristics include a versatile and uncomplicated sensor design, remote sensing capabilities, ongoing analysis, and in situ monitoring.

Additionally, they exhibit reduced confinement loss compared to previous versions. Furthermore, traditional optical fibers can hinder electromagnetic interference, exhibit mechanical stability, and result in little confinement loss within the optical spectrum. SPR sensors based on PCFs have recently received higher acceptance than conventional fiber because

of their controllable light-guiding mechanism, strong birefringent properties, and highly flexible structural design [55].

The PCF’s small and light construction makes the sensors smaller, thus increasing their suitability for remote sensing. The plasmonic metal coating can be applied on the fiber surface's exterior or within the air holes. Light is fed into the system from one end, and the resulting optical response is observed from the opposite. To achieve a strong connection between the SPP mode and the core mode, we can enhance the design of the PCF, resulting in improved sensing performance. Various renowned plasmonic materials, including graphene, silver, copper, gold, and titanium nitride, are employed to stimulate surface plasmon resonance (SPR). Gold (Au) and silver (Ag) are the predominant choices for plasmonic materials. Gold (Au) is chemically inert, compatible with biological systems, and induces a significant shift in wavelength. Silver produces a more distinct resonance peak compared to gold. In humid settings, oxidation occurs and hampers the precision of the detection procedure.

Consequently, gold is utilized in a more significant proportion of the task. SPR technology encompasses two distinct sensing processes. For internal sensing, the analyte occupies the air holes, while the analyte is positioned on the sensor's surface for external sensing. Regrettably, this technique is impractical for dispersed and real-time sensing due to the requirement of altering the analyte during measurement. Furthermore, evacuating and replenishing the designated air apertures is challenging. In addition, fabricating internal sensing SPR sensors is challenging because they suffer from significant propagation loss.

5.2) Structural Design and Theoretical Modelling-

This paper presents a revolutionary gold-coated PCF SPR sensor that utilizes external sensing. The device can be utilized within the optical to near-infrared wavelength range, specifically between 0.42 and 1.0 micrometers. In the near-infrared range, the evanescent field can penetrate deeply, leading to enhanced detection capabilities. Additionally, affordable laser sources are readily accessible in the market. We have implemented a circular-shaped core structure to facilitate coupling and enhance the overall sensing performance. The objective is to achieve a broad detection range (RI 1.21-1.4) in a sensor that can be readily manufactured. The fiber's outside is coated with a layer of gold, ensuring direct contact between the plasmonic surface and the analyte. To attain the desired level of performance, we enhance the geometric characteristics of the system by optimizing factors such as the radius of the air holes, the distance between air holes that is pitch, the gold layer's thickness, and the analyte layer's thickness.
A circular-shaped lattice structure is proposed. The structure has a simple geometrical arrangement. A circular air hole-based circular-shaped cladding Photonic crystal fiber is proposed in a silica (SiO_2) substrate. Different air hole diameters have been used to shape the cladding. We optimize the air hole diameters, gold layer thickness (tg), and analyte layer thickness (ta) to obtain the optimum conditions. The outer layer is a perfectly matched layer with a thickness of 1.4um to avoid reflections of electromagnetic waves at the interface.
The following steps are used for design criteria
1. PCF Structure: PCF structure that enables efficient light direction and analyte interaction is selected. To enable the excitation of surface plasmon polaritons (SPPs) at the sensing interface, the PCF should have a periodic pattern.
2. Material Properties: Materials that have appropriate dispersion properties and refractive indices is chosen. To guarantee effective detection, the material used in the sensing layer needs to have a high affinity for the target analyte.

3.Excitation Source: Excitation wavelength that corresponds to the SPR sensor's resonance state is chosen. The wavelength at which changes in refractive index cause the greatest sensitivity should match this one.

4. Boundary Conditions: To simulate how light interacts with the PCF and the sensor layer, proper boundary conditions have been applied. To reduce reflections, perfectly matched layers (PML) or other absorbing boundary conditions must be used.
5. Mesh: To precisely capture the characteristics of the sensing layer and the PCF structure, a fine mesh has been used.
6. Sensitivity Analysis: Sensitivity analysis has been used to determine which parameters are most important in determining the performance of the sensor.

Wavelength Sensitivity

It refers to the change in peak wavelength due to a change in RI of the analyte. The following equation calculates WS. As the gaps between the peaks increase WS also increases.

$$S_w = \frac{\Delta\lambda peak}{\Delta na}$$

Amplitude Sensitivity

It refers to the change in confinement loss due to a change in analyte divided by confinement loss at that point.

$$S_A(\lambda) = -\frac{1}{\alpha(\lambda, na)} \frac{\delta\alpha(\lambda, na)}{\delta na}$$

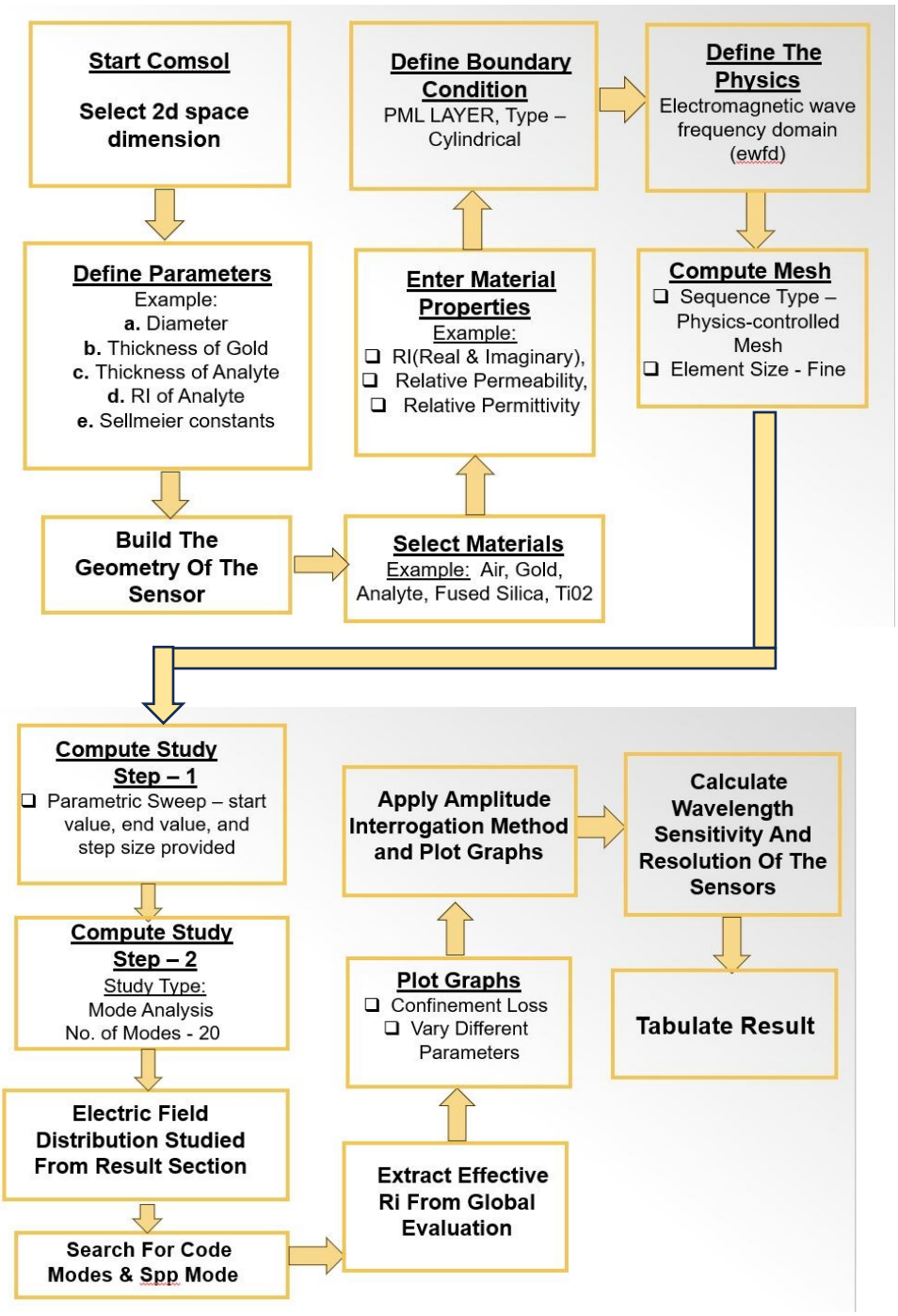

Figure 5.2- Steps that has been carried out in FEM based COMSOL software for structural design and simulation.

5.2.1) Perfectly matched layer

A Perfectly Matched Layer (PML) is a computational tool employed in numerical simulations, such as finite element or finite difference methods, to efficiently absorb outgoing waves and eliminate reflections at the limits of the simulation domain. It is frequently used in simulations of wave propagation difficulties, particularly in the fields of optics and photonics.

When simulating a biosensor using a photonic crystal fiber (PCF), employing a Perfectly Matched Layer (PML) can be advantageous in reducing undesired reflections at the boundaries of the simulation area, guaranteeing that the simulated environment behaves as if it were infinite. Accurately modeling the behavior of light within the PCF structure is essential for producing realistic results. Below is a comprehensive framework for implementing a PML in a simulation:

Provide a precise definition of the simulation domain: Configure the simulation domain to accurately depict the photonic crystal fiber and its immediate environment.

Enclose the simulation domain with a perfectly matched layer (PML). The purpose of this layer is to absorb outgoing waves effectively, preventing any reflections from occurring within the simulation area.

Adjust PML parameters: Adjust the parameters of the Perfectly Matched Layer (PML) to align with the specific properties of the waves in your simulation. This may require modifying the thickness and absorption characteristics of the PML layer.

Resolve the simulation: Employ numerical methods, such as the finite element method or finite difference approach, to solve the wave propagation equations inside the simulation domain.

Evaluating Findings: Analyze the outcomes inside the PCF framework while ensuring that reflections from the borders do not disrupt our analysis.

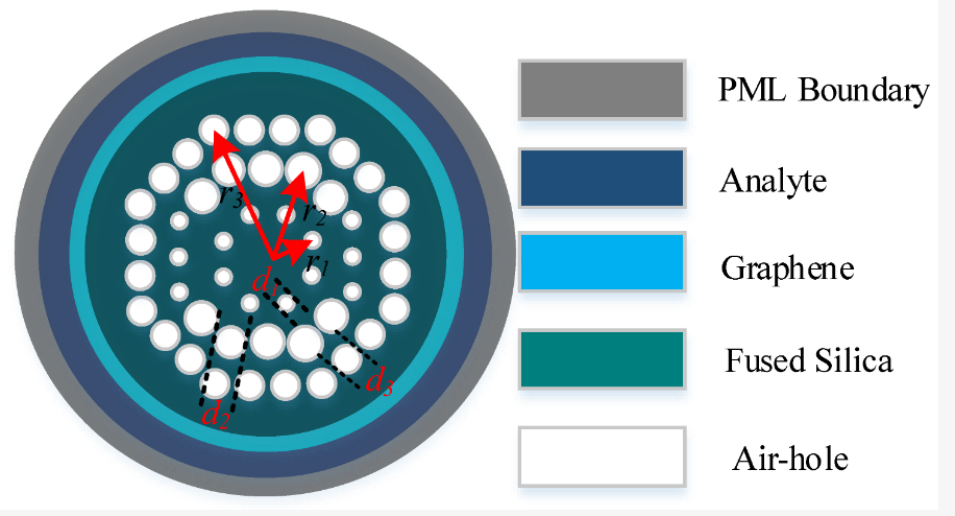

Figure 5.2.1-Illustration of PML is utilized to provide a high level of fidelity between the simulated environment and real-world conditions. This is achieved by reducing the presence of spurious reflections that may occur at the boundaries of the simulation [56].

5.3) Cross-sectional layout

In the cladding region, fifteen circular-shaped air holes have three different diameters. The two largest air holes on the top and bottom of the fiber center have a diameter of 1.6um, as denoted by d3. The three smallest air holes to the cladding structure's left, right, and center have a diameter of d1 equal to 0.4um. The ten air holes on the outer part of the cladding adjacent to the gold layer have a diameter of 0.8um and are denoted as d2. A gap between subsequent air holes is created to maintain electromagnetic flow toward the metal. Adjacent to the PML is the layer through which we will pass biochemical analyte for detection. This is termed as ta. The thickness of this layer is selected to be 35um. 40nm thickness of the gold layer is placed along the analyte layer.

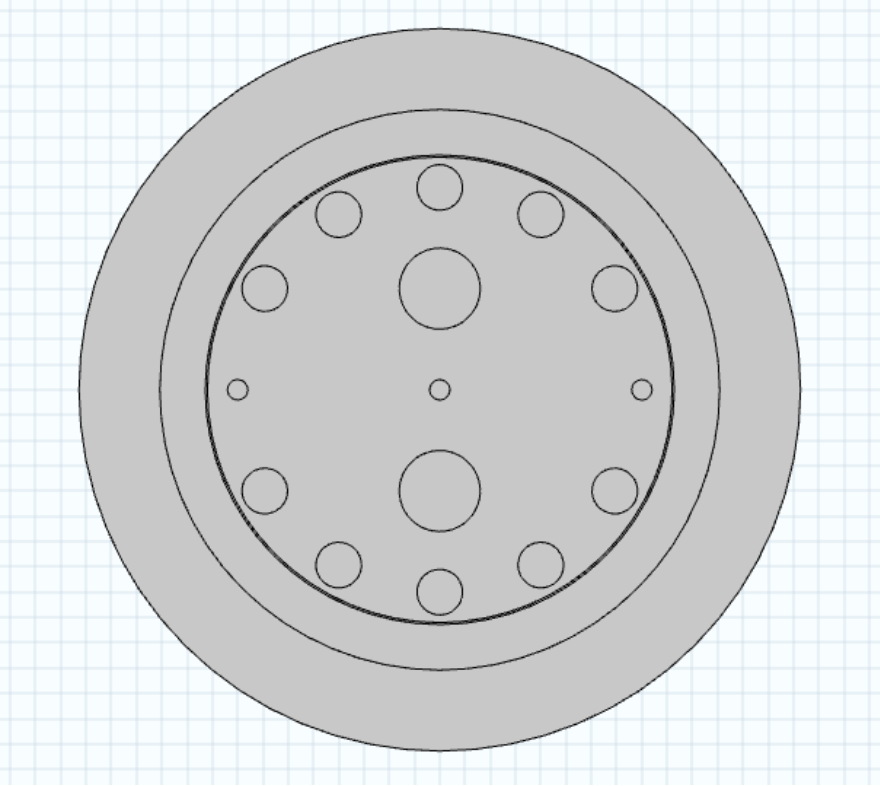

Figure 5.3- Cross section of the proposed design 1. An array of circular air holes creates a dual core where light can be confined. A thin layer of gold is used as plasmonic material. The sensor is based on a Silica substrate whose material dispersion is calculated by the Sellmeier Equation. Material dispersion of gold is calculated using the Drude-Lorentz model.

Plasmonic materials such as gold exhibit strong interactions between light and free electrons, leading to SPR. SPR is highly sensitive to changes in local RI, making gold useful for sensing applications. Gold has high RI sensitivity. This property is exploited in plasmonic sensors where shifts in resonance wavelength are used to detect changes in the local environment. Gold has low absorption loss near the IF region. It is a chemically stable material. This is important because the material may come in contact with different environments in sensing applications. Gold nanoparticles ensure enhanced light-matter interactions because of strong field confinement at the nanoscale.

5.3.1) Pitch

The pitch of a PCF is the precise measurement of the distance between the centers of two neighboring air holes inside the fiber's periodic structure. The pitch is a fundamental factor in determining the optical features of the PCF and plays a significant role in defining its qualities.

The pitch of a PCF is one of the design characteristics that influence the guiding qualities of the fiber, along with factors such as the diameter of the air holes and the refractive indices of the materials used. By manipulating these parameters, designers can regulate the direction of light within the photonic crystal fiber (PCF), resulting in distinctive optical characteristics that differentiate PCFs from conventional optical fibers.

PCFs with varying pitch values can be selected according to the specific optical properties and intended uses.

5.3.2) Photonic Bandgap Guidance:

In the context of a PCF, a Photonic Bandgap (PBG) refers to a specific range of wavelengths where the fiber's core substantially restricts or completely prevents light propagation. The periodic organization of air holes or other materials with low refractive index in the PCF cladding area causes the occurrence.

Within the bandgap region, specific wavelengths of light are prohibited from propagating through the fiber's core. The periodic structure of the fiber induces destructive interference for those particular wavelengths, thereby impeding their transmission through the fiber.

Within the bandgap, some wavelengths can be directed through the core of the PCF. The guided modes can propagate without encountering substantial loss.

The periodic arrangement of PCFs can generate bandgaps in the photonic band structure, enabling the fiber to direct light distinctly compared to traditional fibers. The pitch determines the position and breadth of these bandgaps.

The pitch also influences the restriction of optical modes within the fiber. Reducing the size of the pitches can lead to enhanced mode confinement, affecting the effective mode area and other

optical characteristics. All the air holes' centers are at a distance of 2×p from the fiber's geometric center.

5.4) Guiding Properties and Dispersion Characteristics

X and Y polarization modes

The figure shows light energy allocation for core mode and SPP mode. At analyte RI 1.36, energy distribution for core mode X and Y polarization is displayed. The X polarization core mode has its electric field vector primarily facing along the x direction, and the Y polarization core mode has its electric field vector oriented towards the Y direction. The oscillation of the electromagnetic wave associated with X mode is in the horizontal direction, and Y mode is in the vertical direction.

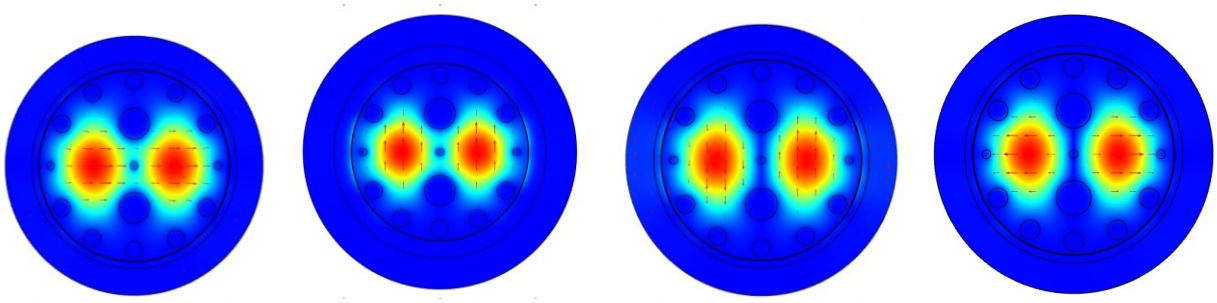

Figure 5.4 - Even and odd X and Y polarization core modes.

5.4.1) SPP modes

SPP modes refer to the mode that involves coupling of photons with surface plasmon oscillations along the interface between metal and die electric regions within PCF. Gold is used to support SPP mode. The sensing performance is determined mainly by the SPP modes [57]. Surface plasmon polaritons are electromagnetic modes with a locally enhanced electric field [58].

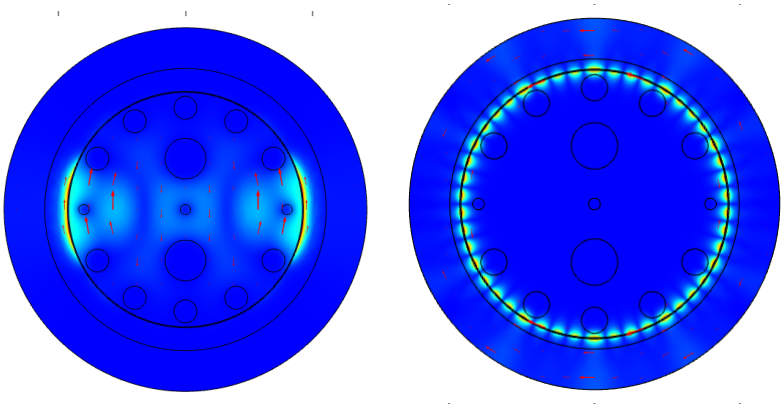

Figure 5.4.1- SPP modes for optimized parameters

5.5) Sensor performance analysis and optimization of different parameters

5.5.1) RI Optimization

It involves varying the design parameters to achieve the best sensitivity and performance. The sensor's sensitivity can be improved by optimizing the design to support specific modes. Surface functionalization, numerical simulation, experimental validation, and temperature considerations are some steps that can be followed for RI optimization. The wavelength is varied by a parametric sweep in COMSOL to obtain the confinement loss curve from 0.45um to 1um. Confinement loss is calculated by increasing the RI of the analyte from na= 1.21 to 1.24 and again from 1.31 to 1.40 with an increment of 0.01. Wavelength variation for na= 1.31 to 1.35 is 0.51um to 0.71um with increment of 0.01um. Wavelength variation from 1.36 to 1.40 is from 0.5um to 0.89um with an increment of 0.01um. The confinement loss for Y polarization is stronger than for X polarization for the proposed sensor, so we study Y polarization mode only. The following equation calculates the confinement loss

$\alpha = 8.686 \times k_o \times Im[neff] \times 10^4 dB/cm$ where $k_o = \frac{2\pi}{\lambda}$, Im[neff] is the imaginary part of the effective refractive index.

Figure 5.5.1a, b shows the proposed sensor's confinement loss and amplitude sensitivity depending on the wavelength with different RI of the analyte. From the loss curves, a maximum

loss of 588db/cm occurs at na=1.40, and a minimum loss of 100db/cm occurs at na=1.36, according to Figure 5.5.1c. 148dB/cm, 228dB/cm, and 355dB/cm loss occurs at na= 1.37, 1.38, 1.39, respectively. Figure 5.5.1b,d,f shows amplitude sensitivity corresponding to the variety of RI of the analyte. Amplitude sensitivities are $393RIU^{-1}$, $616RIU^{-1}$, and $920RIU^{-1}$ with RI of analyte na=1.36, 1.37, and 1.38. The highest AS is achieved at $1096RIU^{-1}$ for na=1.39.

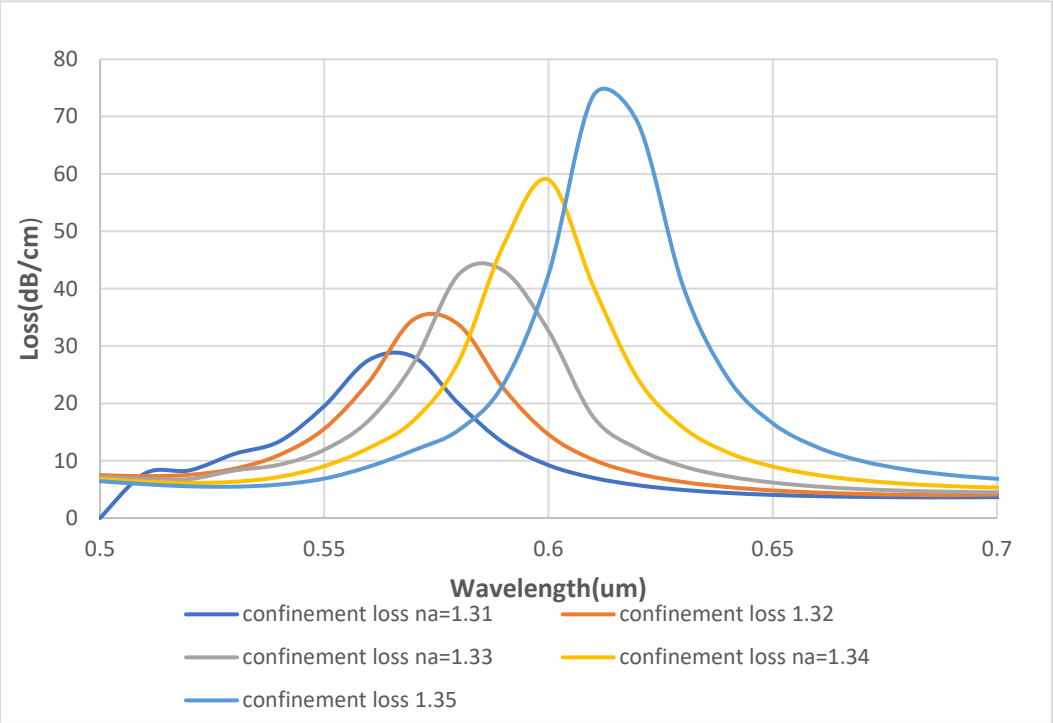

Figure 5.5.1a - Loss curves by varying the refractive index of the analyte from 1.31 to 1.35

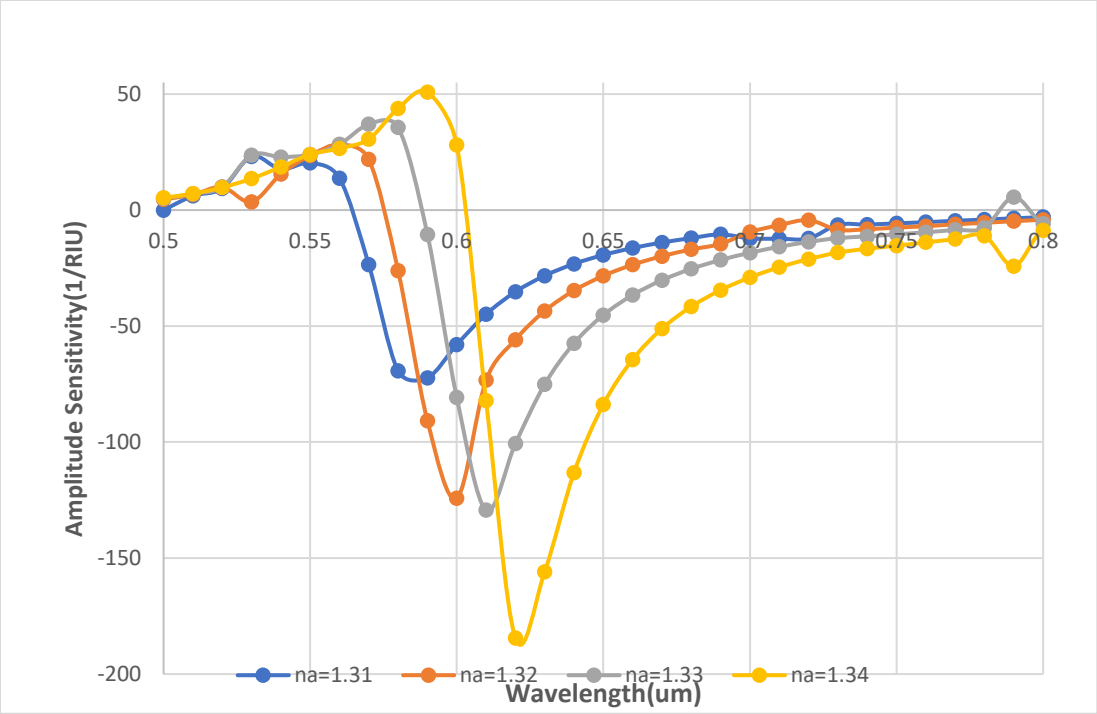

Figure 5.5.1b- Amplitude sensitivity for analyte na= 1.31 -1.34.

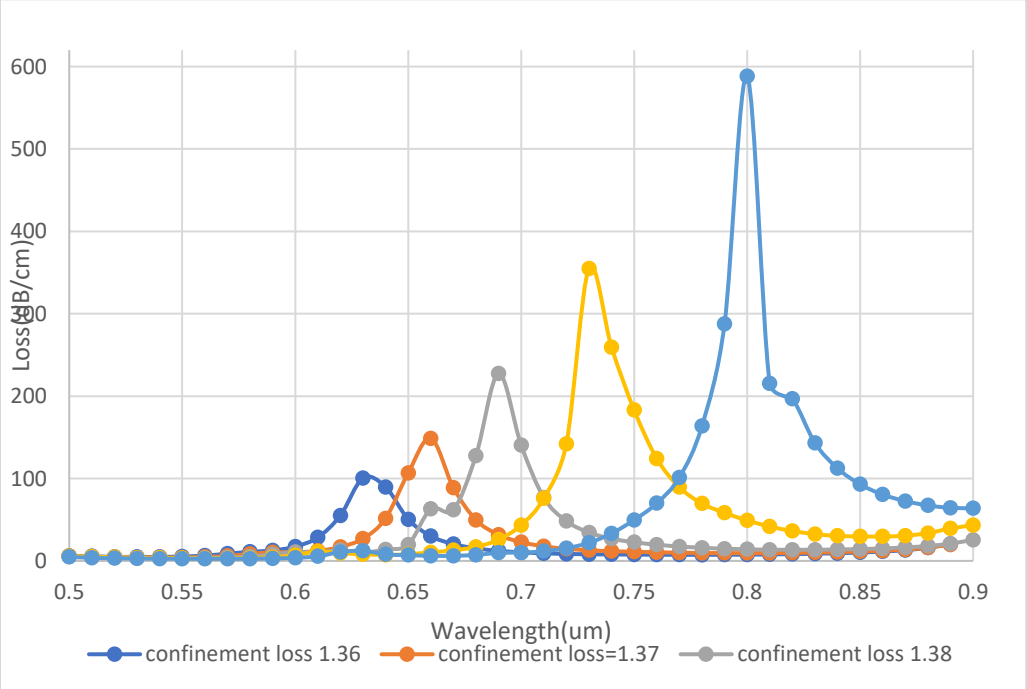

Figure 5.5.1c- Loss curves by varying analyte's refractive index from 1.36 to 1.38.

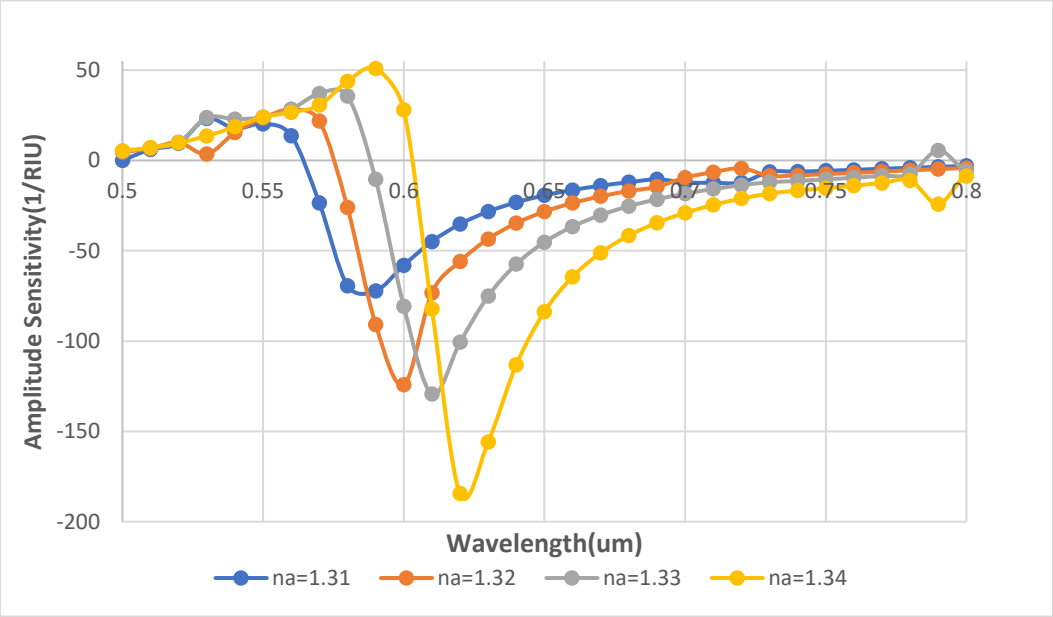

Figure 5.5.1d- Amplitude sensitivity for analyte na= 1.31 -1.34

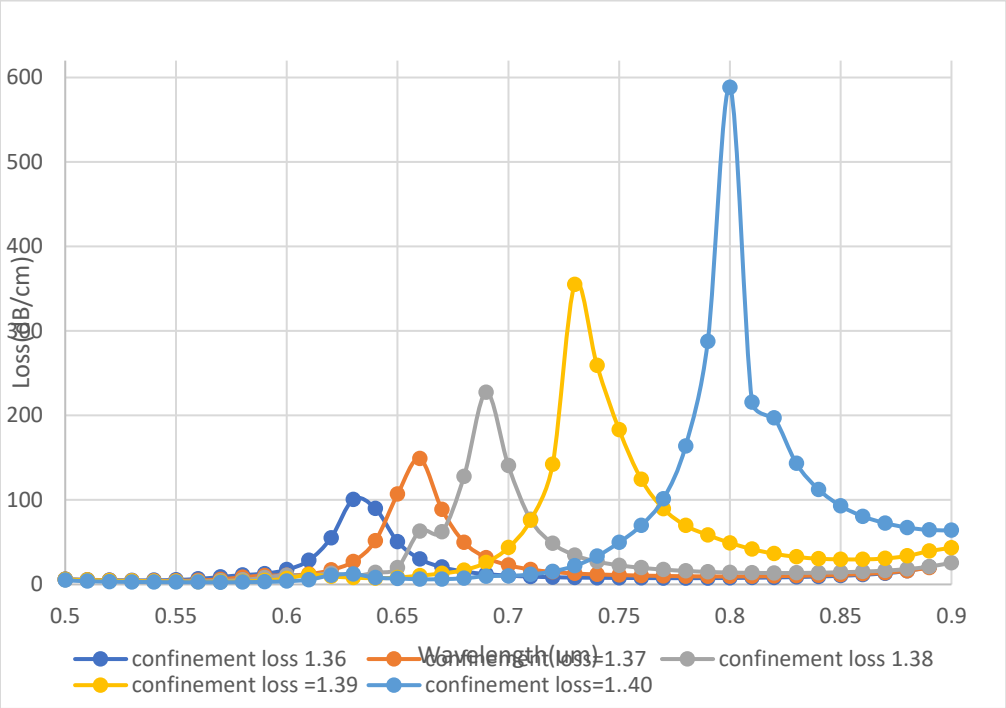

Figure 5.5.1e - Loss curves by varying analyte's refractive index from 1.31 to 1.

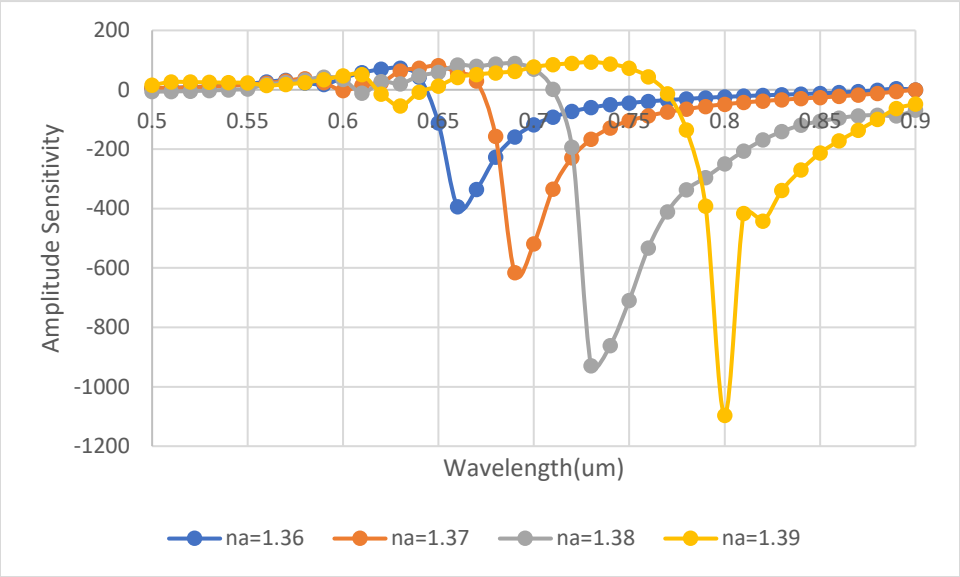

Figure 5.5.1f- Amplitude sensitivity for analyte na= 1.36 -1.39

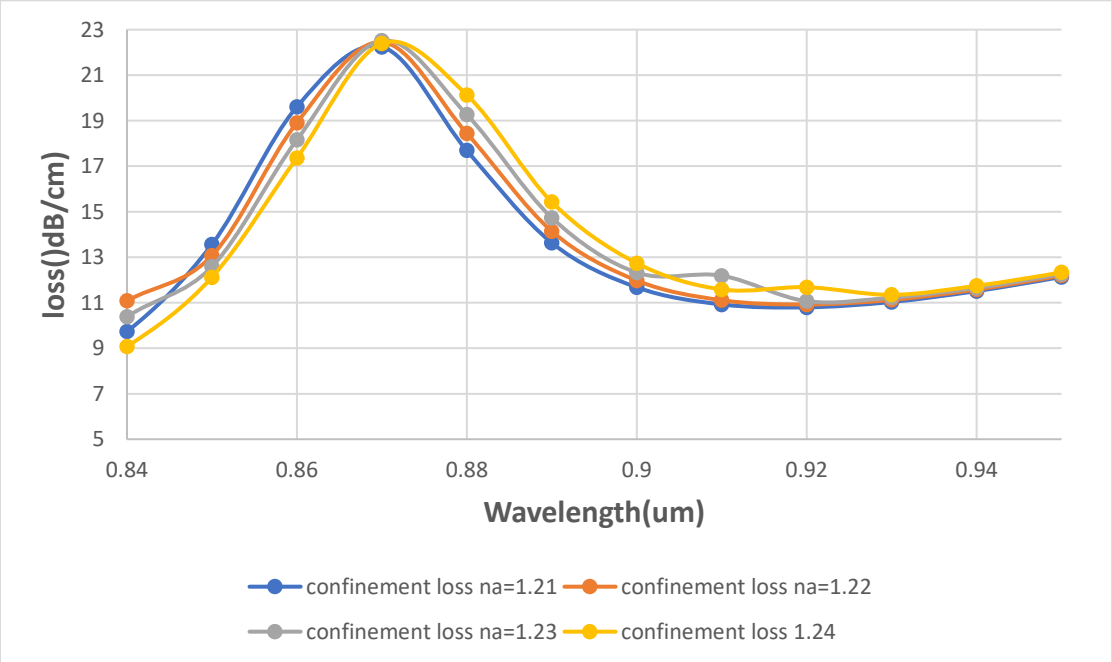

Figure 5.5.1g - Loss curves by varying the analyte's refractive index from 1.21 to 1.24.

5.5.2) Air Hole diameter optimization

The air holes result in birefringence by creating asymmetry in the design, leading to different RI for different polarizations. Varying air hole parameters in PCF influence how light is guided within the fiber. Changing air holes' size, shape, and arrangement leads to bandgap engineering. The location and width of the photonic bandgap in the PCF's optical spectrum can be controlled. Varying air hole diameter also allows control over modal properties such as mode confinement, effective RI, and dispersion characteristics. Also, polarization control and engineering of fibers to support specific polarization modes is possible by varying air hole diameter. It can also make PCF sensitive to external parameters such as RI, temperature, or strain.

Moreover, the dispersion characteristics of PCF can be tailored by varying air hole dimensions, which is vital in supercontinuum generation, where dispersion characteristics are essential for broadening the spectrum of guided light. Better fabrication tolerance can be achieved by variation of air holes. Fig 5.5.2a shows the variation of air hole diameter d1=1.6um, 1.8um, and 2um at RI of analyte na=1.36. Loss peaks are obtained at 98dB/cm for 1.6um and 29.64dB/cm for 1.8um. Next, na is changed to 1.38, and d1 is varied. At d1= 1.8um, a 35.88dB/cm loss peak is obtained, and at d1=2um, a 38.7dB/cm loss peak is obtained. Figure =5.5.2b shows that when air hole diameter d2=0.6um gives a high loss peak of 156dB/cm, d2=1um yields 89.3dB/cm loss peak, and d2=0.8um results in confinement loss of 89.7dB/cm.

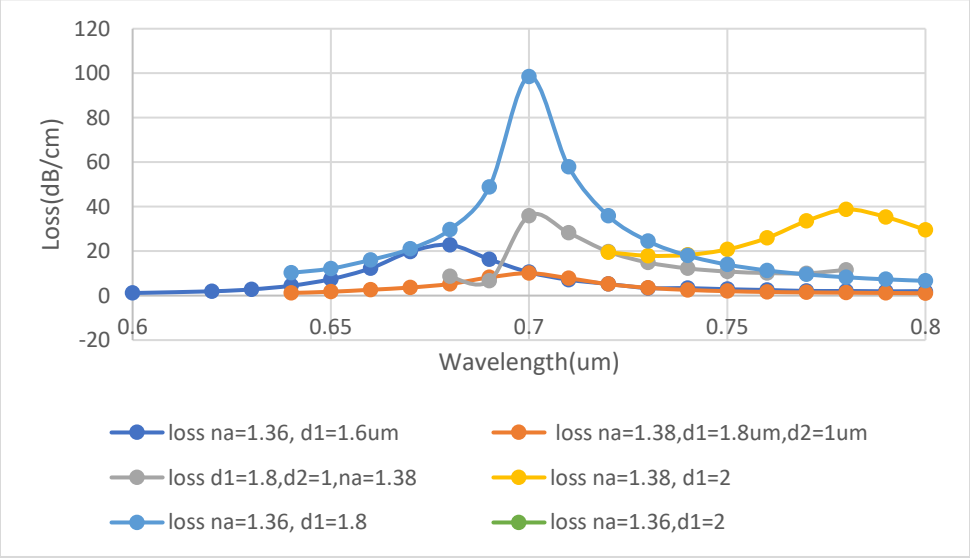

Fig5.5.2 a– loss curves by variation of air hole with diameter d1

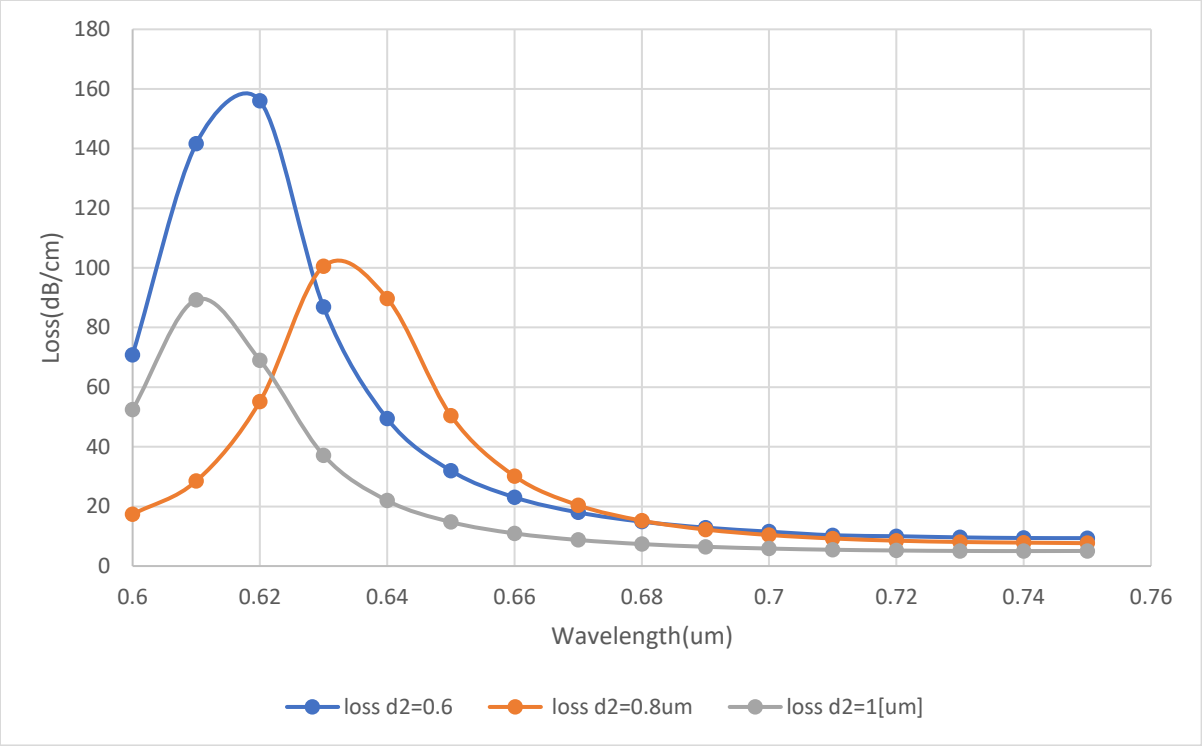

Fig 5.5.2b- Confinement loss by d2 variation

5.5.3) Gold layer thickness Variation

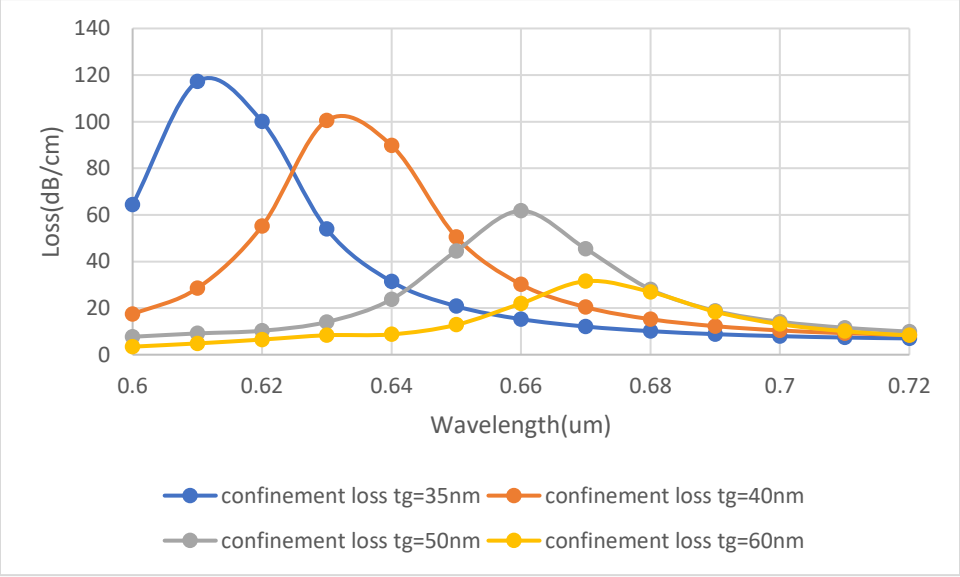

Fig5.5.3 a- confinement loss for variation of gold layer thickness

Varying the thickness of the gold layer in PCF substantially influences the plasmonic characteristics and sensing capabilities of the fiber. The thickness of the gold coating affects the

parameters for SPR. SPR refers to the coordinated vibrations of electrons at the boundary between a metal and a dielectric material. SPR happens when the momentum of incoming light aligns with that of surface plasmons. The thickness of the gold layer influences the resonance state.

RF Sensitivity

SPR has a high level of sensitivity towards variations in the refractive index of the adjacent medium. By adjusting the gold layer's thickness, the PCF sensor's sensitivity to variations in refractive index may be enhanced. By altering the thickness, one can adjust the resonance wavelength to align with the intended range for detecting particular analytes.Increasing the thickness can enhance the plasmonic responses and result in more significant losses. Ensuring a balance between these parameters maximizes the overall sensing performance.

Obstacles in manufacturing The production of PCF with different gold layer thicknesses may be difficult. Precise control is necessary when employing techniques such as physical vapor deposition or chemical deposition procedures to attain the requisite level of thickness uniformity.

Mode coupling

It refers to the phenomenon where different modes of a system interact with each other, leading to a transfer of energy between the modes. The presence of a gold layer enables the interaction of light with plasmonic modes. Modulating the thickness can impact mode coupling efficiency and distribution of electromagnetic fields within the fiber.

Gold

Au, or gold, has an atomic mass of 196.96657 and a melting point of 1064 °C. Gold is used to cover the exterior of the biosensor. It is a chemically stable and inert compound. It does not get oxidized in an aqueous environment. Gold undergoes a sharp and broad resonant peak in an aqueous environment. The Drude-Loretz model gives a dielectric constant of gold, as shown below.

$$\varepsilon_{Au} = \varepsilon_{\infty} - \frac{{\omega_D}^2}{\omega(\omega + j\gamma_D)} - \frac{\Delta\varepsilon \cdot {\Omega_L}^2}{({\omega^2} - {\Omega_L}^2) + j\Gamma_L\omega}$$

In this equation, εAu represents the permittivity of gold, and ε∞ represents the high-frequency permittivity with a value of 5.9673. ω is the angular frequency, ωD and γD are plasma and

damping frequencies, respectively, where ωD = 4227.2π THz, γD = 31.84π THz. Moreover, Δε = 1.09 is the weighting factor, while the oscillator strength is ΩL = 1300.14π THz, and the spectral width is ΓL = 209.72π THz[12].

Figure 5.5.3a displays the shift in resonance wavelength as the thickness of the gold layer is varied. The wavelength varies from 0.6 µm to 0.72 µm, while gold thickness is varied at 35 nm, 40 nm, 50 nm, and 60 nm. A thicker gold layer results in greater surface electrons, improving sensitivity. On the other hand, thickness may reduce the sensitivity as it restricts electromagnetic waves from interacting with the analyte layer. The sensitivity decreases as gold layer thickness increases, as shown in Figure 5.5.3b. This is due to the high damping loss of gold. We selected 40 nm as the optimized value of gold, where sensitivity is equal to 122.7RIU^{-1}.

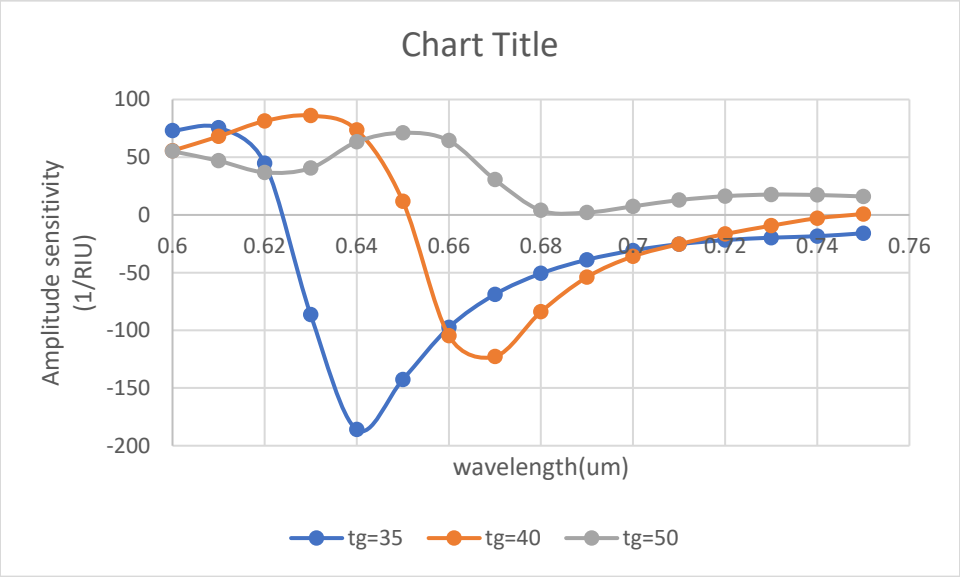

Figure 5.5.3b- Amplitude sensitivities for variation of gold layer thickness.

5.5.4) Variation of Analyte layer thickness

The analyte layer, which comes into contact with the target molecules, is crucial in determining the sensor's sensitivity, response time, and overall effectiveness. The thickness of this layer has a direct impact on these factors. Below are some factors to consider and processes to follow to adjust the thickness of the analyte layer in a photonic crystal fiber (PCF) biosensor:

Comprehend the Mechanism of Sensing:

PCF biosensors can function via different sensing techniques, including variations in refractive index, surface plasmon resonance, or modifications in guided modes. In this paper, the SPR sensing technique is used.

Examine the characteristics of the analyte:

The properties of the target analyte, such as its dimensions, electrical charge, and molecular mass, can influence its interaction with the PCF surface. Consider these characteristics when choosing the most suitable thickness for the analyte layer.

Select Appropriate Materials:

Choose materials for the analyte layer suitable for photonic crystal fiber (PCF) and the target molecules. Consider variables such as compatibility with living organisms, the ability to remain unchanged over time, and the capability to fixate the substance being analyzed on the surface of the photonic crystal fiber (PCF).

Precision Manufacturing Methods:

Employ precise manufacturing methods to apply or fixate the layer of the analyte onto the surface of the PCF. Depending on the analyte's characteristics and the photonic crystal fiber (PCF) surface, various methods such as chemical vapor deposition, self-assembly, or layer-by-layer deposition can be used.

Computational simulations involving numerical methods:

Utilize numerical simulations, such as finite element analysis or finite-difference time-domain simulations, to simulate the interaction between light and the analyte layer. Simulations can be utilized to forecast the sensor's reaction to various thicknesses of analyte layers. In this paper, analyte layer thickness ta varies at 0.35, 0.55, 0.65, and 0.75. A distinct peak is obtained at 0.35um thickness, while there is little peak change for the other thickness values. Therefore, ta=0.35um is considered the optimum value.

Maximize sensitivity:

Conduct trials using various thicknesses of the analyte layer to determine the ideal thickness that maximizes sensitivity to variations in the target molecules. Amplitude sensitivity is analyzed for various thickness values.

Take into account multilayer structures.

To optimize the sensor's performance, it is advisable to utilize multilayer architectures, taking into account the sensing method. Extra layers can potentially increase the surface area available for interaction with the analyte or enhance the sensor's selectivity.

Continuous iteration and verification are crucial to guarantee the dependability and precision of the biosensor.

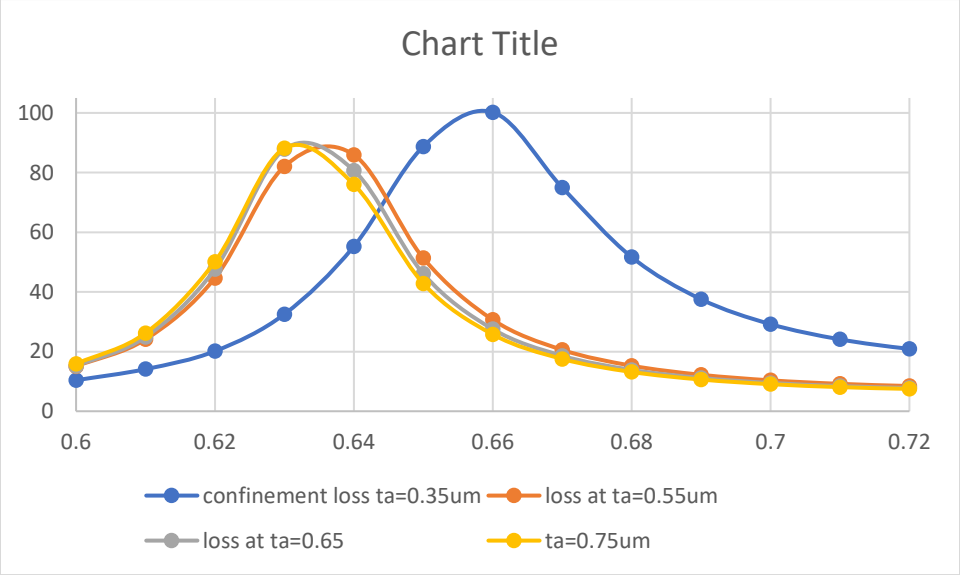

Figure 5.5.4- Loss curves for variation of analyte layer thickness

5.5.5) Variation of pitch

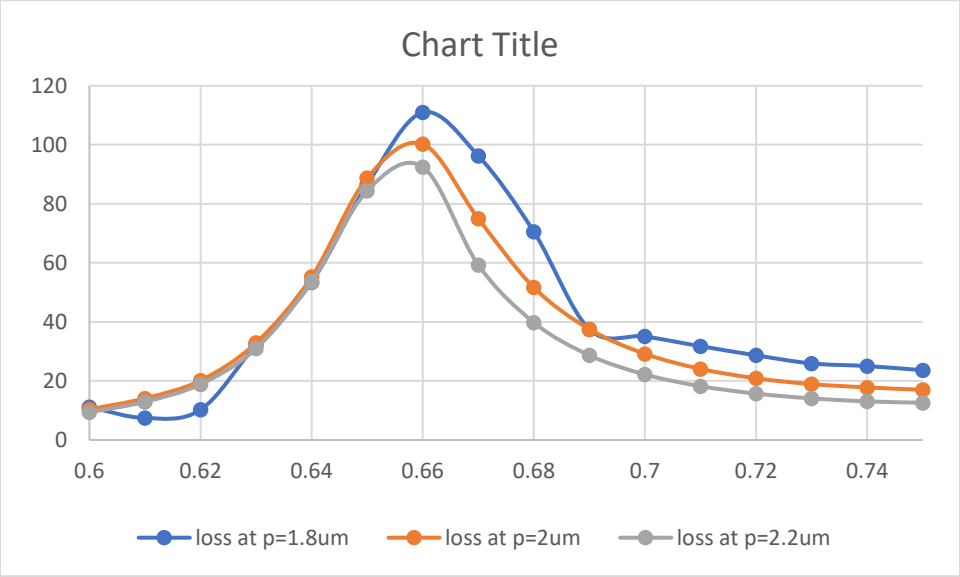

Figure 5.5.5- Variation of pitch size at 1.8um, 2.0um and 2.2um.

As the pitch value is raised, the amplitude of the loss peak reduces slowly. Increasing the pitch resulted in a minor blueshift, specifically shifting the resonant peak towards a shorter wavelength. Based on the coupling level between the core and the SPP mode, the pitch is 2um. A reasonable distance between the air holes and the sensor's center ensures better light confinement.

5.5.6) Phase matching

Phase matching happens when the surface plasmon wave's phase velocity aligns with the incident light's phase velocity. This phenomenon results in the amplification of light-surface plasmon interaction through constructive interference, leading to resonance. When the phase matching requirement is satisfied, the sensitivity of SPR based PCF sensors to variations in the refractive index of the surrounding medium is maximized. Even slight alterations in the refractive index near the metal surface result in noticeable deviations in the resonance state. Engineers and researchers can tailor the design of the PCF, including the structural parameters of the photonic crystal lattice and the metal layer thickness, to achieve specific phase-matching conditions that optimize sensing performance. For the proposed sensor, the effective RI of core and SPP modes intersect at wavelength 0.63um. The real value of both modes becomes equal at 1.4538 with a loss peak at a maximum of 100dB/cm.

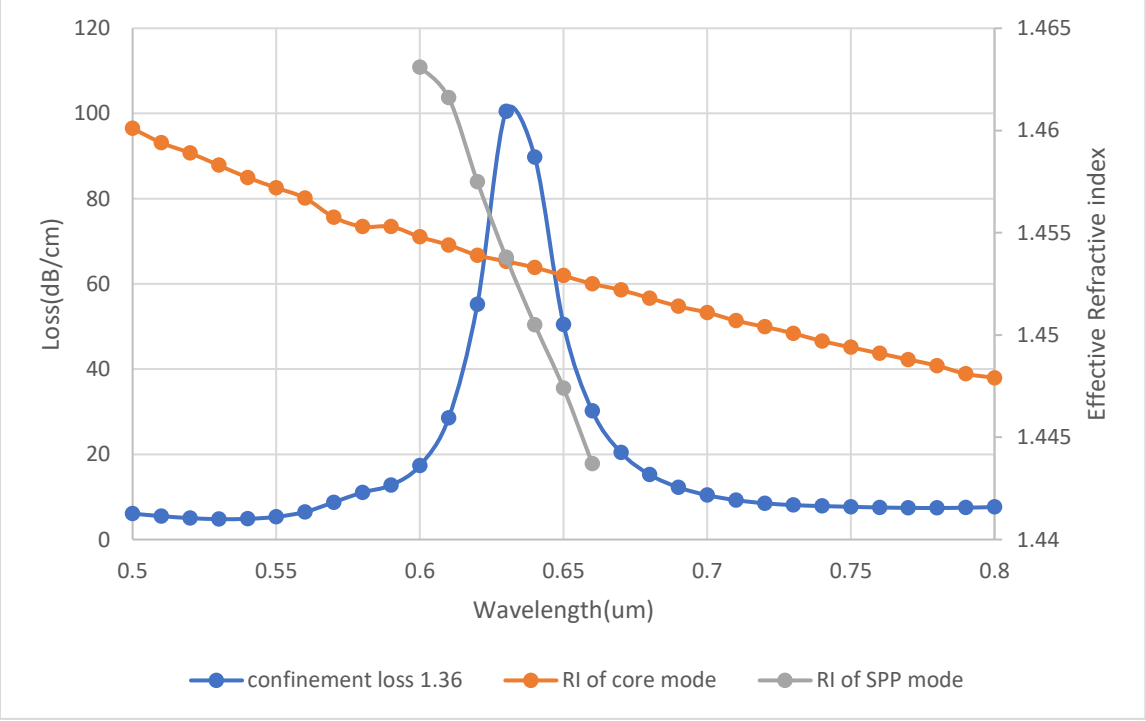

Fig5.5.6-Phase matching condition where RI of SPP mode and RI of core mode intersect for optimized parameters.

5.6) Conclusion

A dual-core PCF SPR biosensor has been investigated with a maximum wavelength sensitivity of 7,000nm/RIU and maximum amplitude sensitivity of 1096RIU^{-1}, taking into account the wavelength and amplitude interrogation approach. The analyte range is 1.21 to 1.24 and 1.31 to 1.40. The maximum resolution is 5×10^{-5}at na equals 1.35. A circular, perfectly matched layer is used to illuminate radiation towards the surface. Given its promising results and straightforward sensing method, the suggested sensor has the potential to be an ideal choice for biological and biochemical analytes.

Chapter 6) Proposed design is a 2-A plasmonic refractive index sensor for detecting low refractive index using a very sensitive dual-core PCF.

6.1) Introduction

The proposed photonic crystal fiber (PCF) is composed of a micro-structured optical fiber that contains a regular pattern of air holes running throughout its whole length. By integrating a metal layer or coating, PCF characteristics can be adjusted to accommodate various modes, such as plasmonic modes.

Plasmon resonance occurs when the guided modes interact with the metal surface. Plasmon resonance is the phenomenon where the energy of the guided mode is linked to the collective oscillations of free electrons at the interface between a metal and a dielectric material. This leads to the amplification of electric fields close to the metal surface.

Plasmonic modes exhibit a high level of sensitivity to variations in the refractive index of the surrounding medium. The sensitivity of plasmonic resonance can be utilized in sensing applications to detect changes in the environment, such as the presence of analytes or fluctuations in temperature, by monitoring alterations in the plasmonic resonance condition.

A plasmonic refractive index sensor for detecting low refractive index is developed using highly sensitive dual-core PCF. Plasmonic material Silver is placed at the edge of the fiber structure to detect changes in the surrounding medium refractive index. A thin titanium dioxide layer is placed on the silver to prevent oxidation. This study presents the design and numerical analysis of a dual-core Photonic crystal fiber(PCF) Surface plasmon resonance sensor developed explicitly for detecting low refractive index. Integrating a microchannel and bimetallic configuration has enhanced the sensing performance in both wavelength and amplitude interrogation methods, creating a dual sensing channel. This occurs due to the generation of significant electrons at the surface when TiO2 is positioned on top of the silver. These electrons attract the field from the core, leading to a strong interaction with the plasmonic mode. Photonic crystal fibers are capable of supporting plasmonic modes. It involves the excitation of surface

plasmons at the metal die electric interface within the PCF structure. The interaction between the guided modes within the fiber and the metal surface results in an increase in light-matter interactions and greater sensitivity to variations in the surrounding media.

6.2) Numerical Design and Modeling

Figure 6.2 illustrates the x-y cross-section of the mentioned sensor. The proposed sensor architecture is organized in a lattice consisting of two layers of air holes. The two air holes (d2) located at the top of the first ring have been reduced in size to enhance the connection between the core-guided and surface plasmon polariton (SPP) modes. To produce a dual-core, two more air holes have been excluded from the center of the initial ring.

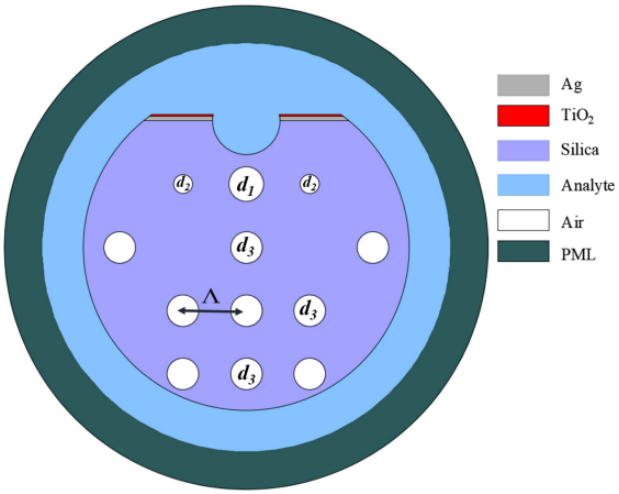

Figure 6.2- Cross section of proposed design 2

Resonance happens when the frequency of the evanescent field aligns with the frequency of the electrons in the plasmonic material. The effective index of the core-guided mode and surface plasmon polariton (SPP) mode coincide at this particular frequency, resulting in a significant increase in confinement loss. The maximum energy is transferred from the core-guided mode to the SPP mode during this moment, which is called the phase-matching condition. The table below shows the confinement loss at wavelengths ranging from 1.5 to 1.76**.** The phase matching

condition occurs at wavelength 1.65um, where the corresponding loss peaks at 263dB/cm. The confinement loss of the sensor is calculated using the following formula:

$$\alpha_{loss} = 8.856 \times \frac{2\pi}{\lambda} \times Im(n_{eff}) \times 10^4 dB/cm.$$

For background material, SiO2 is used, whose refractive index is calculated by the following Sellmeier equation-

$$n_{si}^2(\lambda) = 1 + \frac{B_1\lambda^2}{\lambda^2 - C_1} + \frac{B_2\lambda^2}{\lambda^2 - C_2} + \frac{B_3\lambda^2}{\lambda^2 - C_3}$$

The given equation can define the dielectric constant of TiO2-

$$n_{Tio_2}^2 = 5.913 + \frac{2.441 \times 10^7}{\left(\lambda^2 - 0.803 \times 10^7\right)}$$

6.3) Results and Discussion

6.3.1) Phase Matching condition

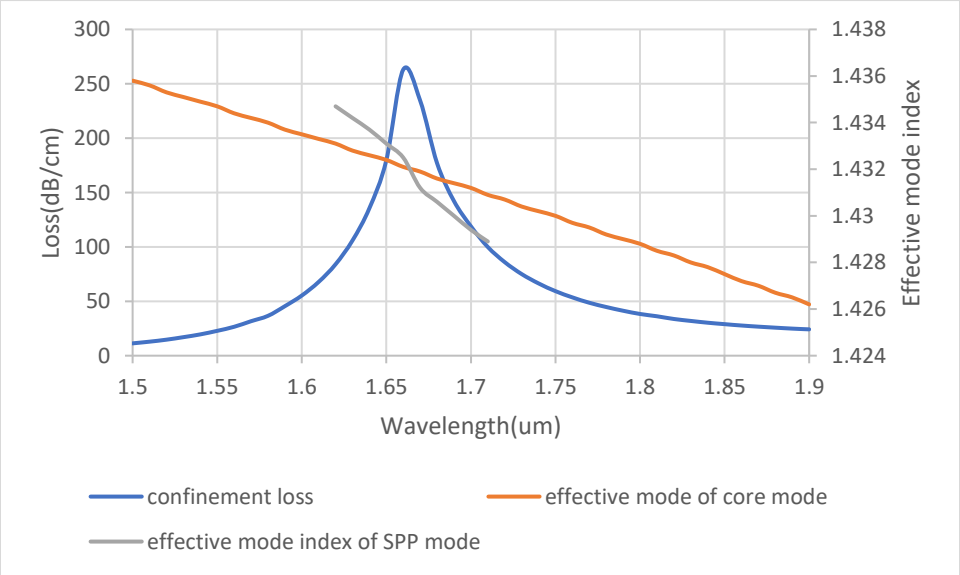

Figure 6.3.1a- Phase matching condition of proposed design 2.

As the phase matching condition is fulfilled, maximum power transfer can be observed from the core-guided fundamental mode to the plasmonic mode. As a result, a peak is observed at the point of intersection.

The figure illustrates the highest amount of energy that may be transferred from the core mode to the surface plasmon polariton (SPP) mode under resonance or phase-matching conditions.

The blue curve represents the loss, while the red line represents the real component of the effective RI of the core mode. In addition, the grey line represents the effective refractive index of the surface plasmon polariton (SPP) mode. The figure demonstrates that the loss of the core mode rises as the wavelength increases until it reaches the resonance point, after which it declines with further increases in wavelength. Conversely, the real component of the effective refractive indices for both the core mode and SPP mode decreases as the wavelength increases. Furthermore, the real part of the core mode's effective refractive index (RI) precisely intersects with the effective RI of the surface plasmon polariton (SPP) mode and fulfills the resonance condition. The figure shows that the resonance takes place at a wavelength of 1.67 μm at an effective RI of 1.4312, and there is an immediate transfer of maximum photon energy from the core mode to the SPP mode. The curve shows a peak loss at 263dB/cm. The resonance condition is essential for the functioning of the suggested sensor as it allows for the effective and precise detection of different analytes utilizing the interaction between the plasmonic material and the photons of the evanescent optical field.

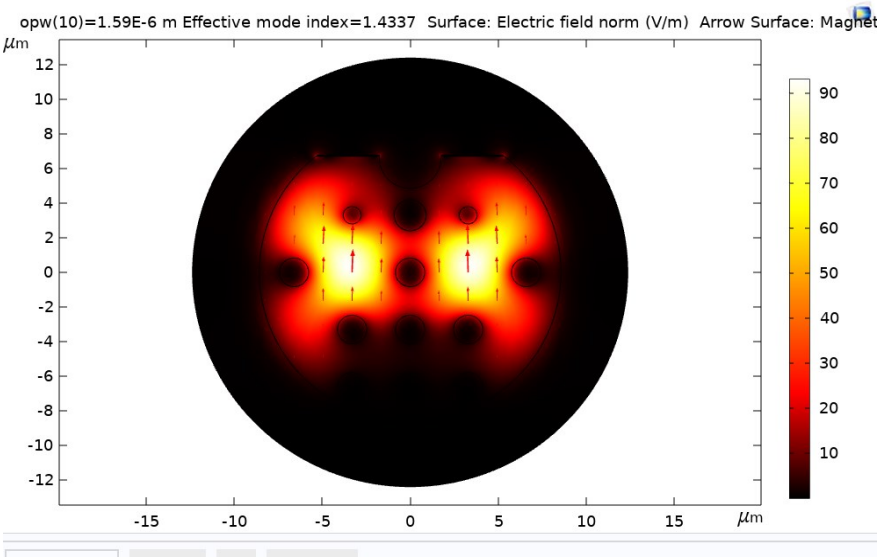

Figure 6.3.1b-Y polarization Core mode of PCF biosensor. Light is confined within the core.

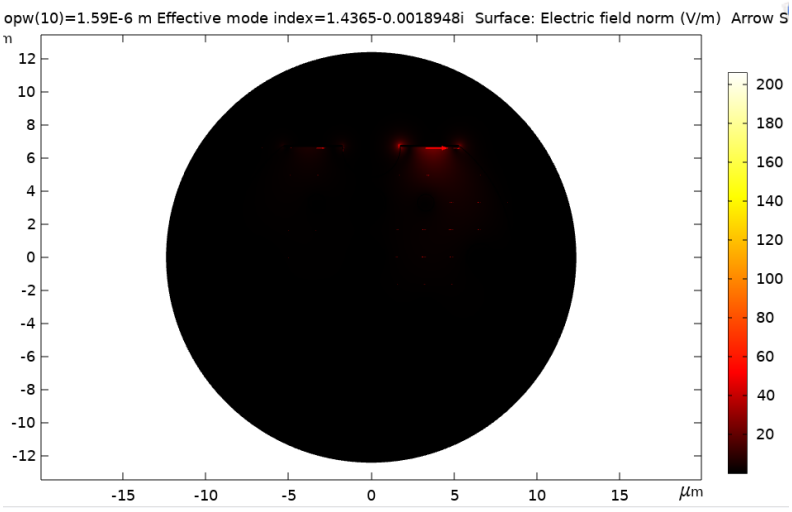

Figure 6.3.1c- SPP mode of the pcf biosensor. The entire field is confined to the plasmonic metal layer.

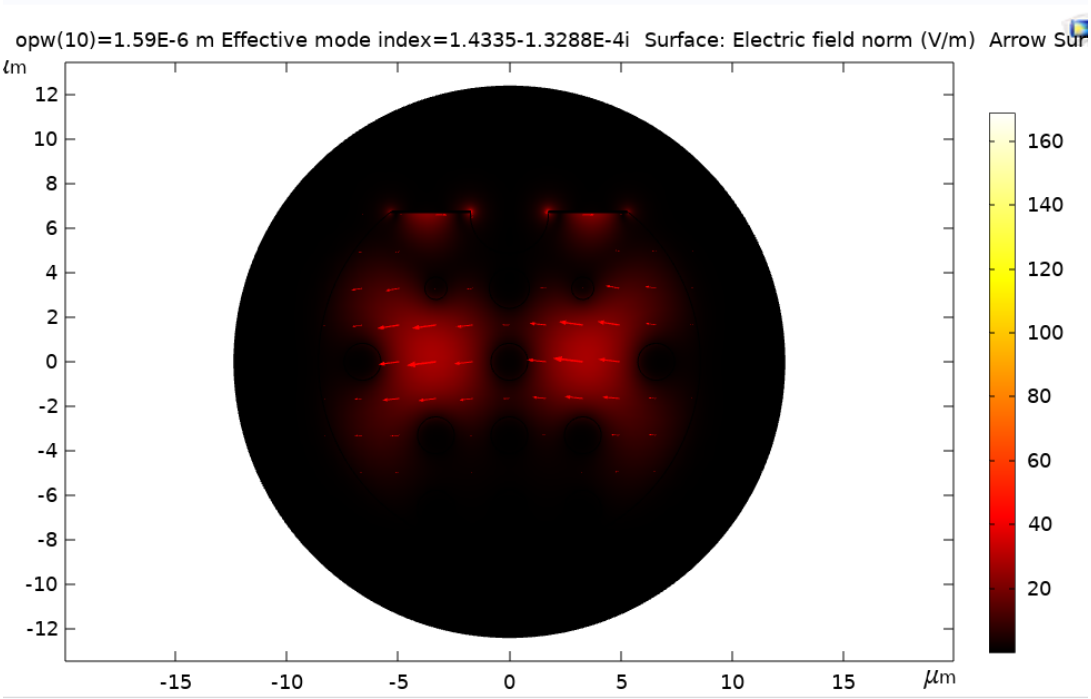

Figure 6.3.1d- SPR mode of PCF biosensor(Resonance condition where the core mode and SPP mode intersect)

6.3.2) RI optimization

In Figure 6.3.2a, the confinement loss and resonance wavelength are represented as functions of the analyte's refractive index. It can be inferred from the figure that as the analyte's refractive index increases, the resonant wavelength shifts towards a higher wavelength. A sharp peak can be obtained at na equals 1.36 with a resonant wavelength of 1.66 micrometers and 263 dB per centimeter peak loss. The peaks slightly decrease as na increases towards a longer wavelength. The analyte's refractive index directly affects the effective refractive index of the guided modes in PCF—increasing na results in higher sensitivity, improving the detection limits of the sensor. High-index materials make interactions with light stronger. This sensor is calibrated by exposing it to analytes with known refractive index. This establishes a relationship between the sensor's response and the analyte's refractive index.

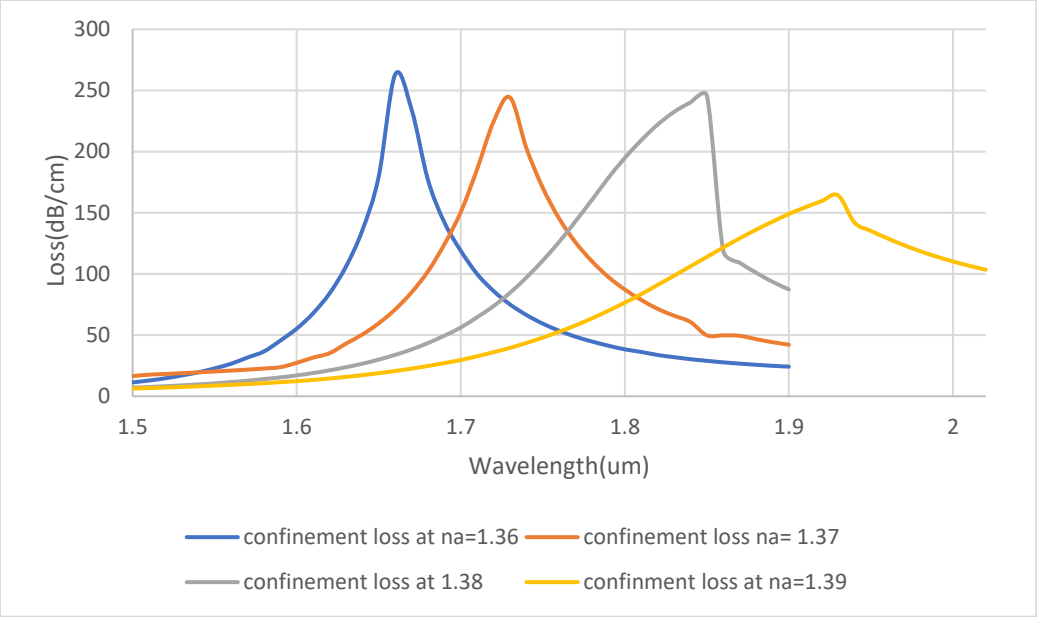

Figure 6.3.2a- Loss curves by varying the refractive index of the analyte from 1.36 to 1.39

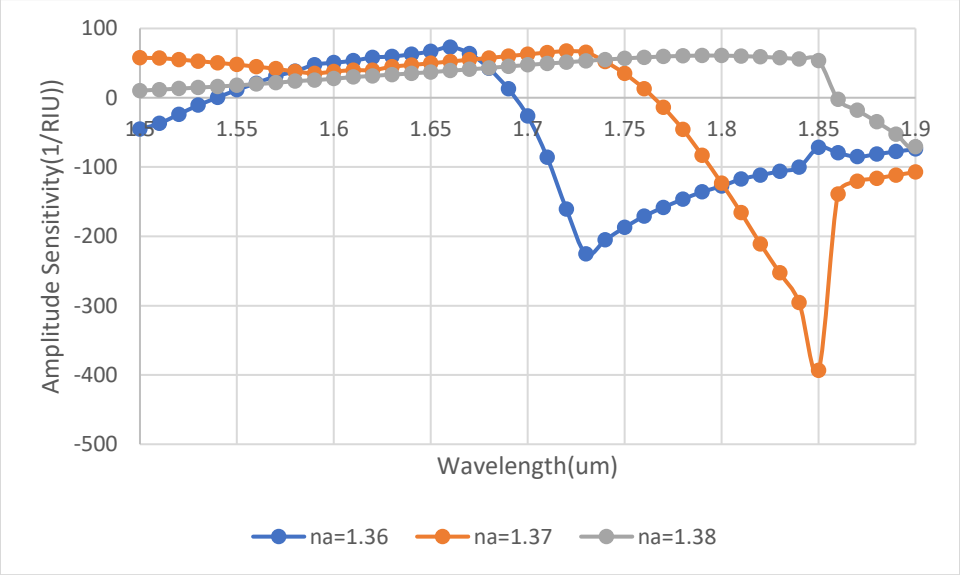

Figure 6.3.2b- Amplitude sensitivity at different na (RI of analyte layer)

6.3.3) Variation of Diameter d1,d2 and d3

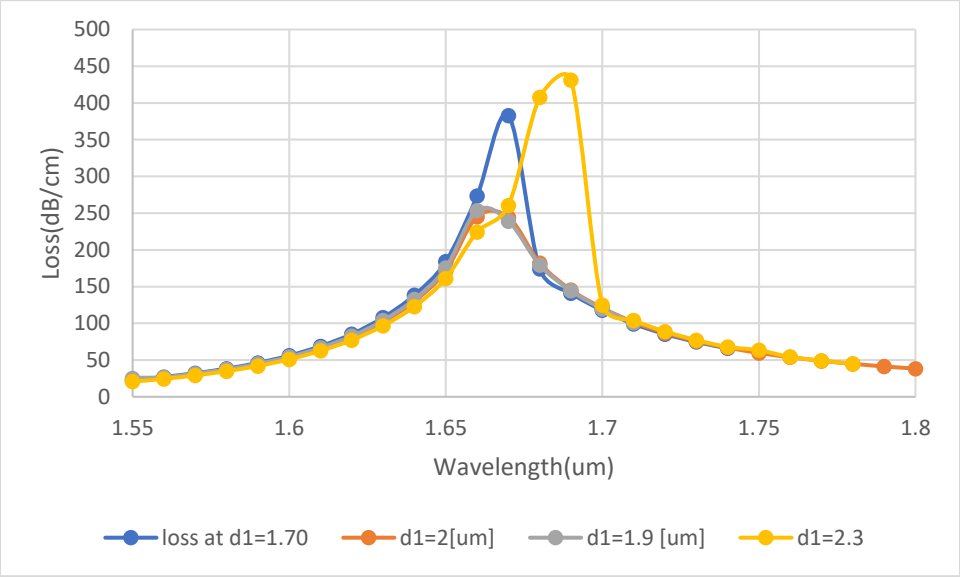

Figure 6.3.3a- Loss curve for variation of d1(Diameter of circle 1)

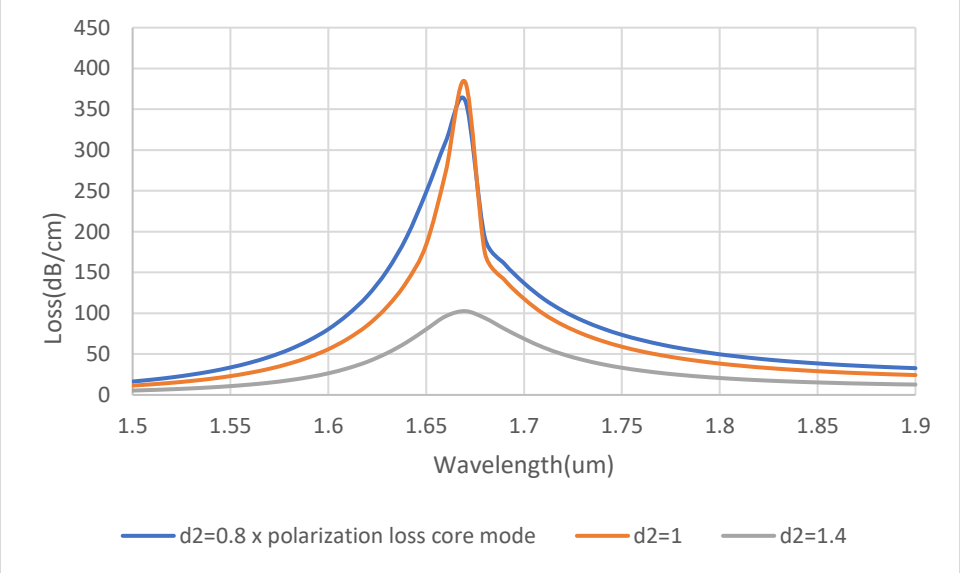

Figure 6.3.3b- Loss curves for variation of d2(diameter of circle 2)

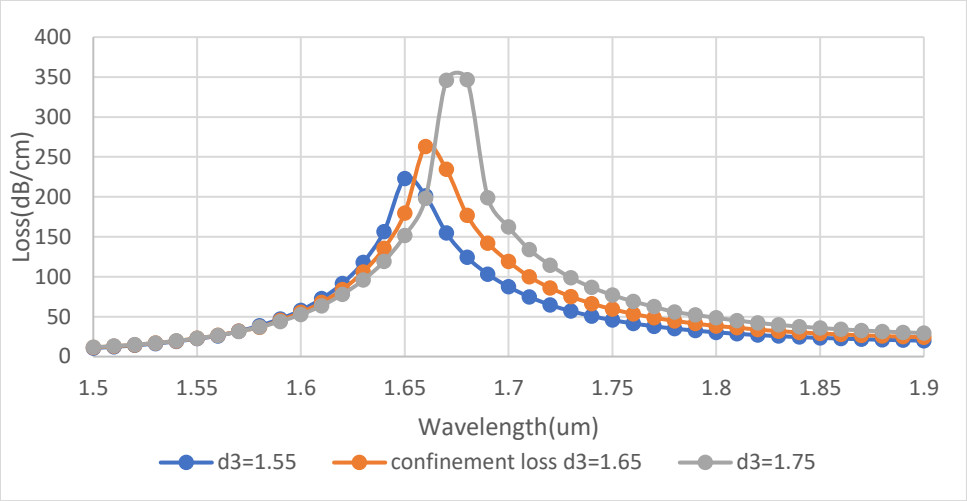

Figure 6.3.3c- Loss curves for variation of d3(diameter of circle 3)

Confinement loss has similar values for 1 µm and 2 µm diameter. As air hole diameter D1 is increased from 1.9 µm to 2.3 µm, the resonant wavelength increases from 1.66 µm to 1.69 µm. The loss peak increases from 253 dB per cm to 431 dB per cm. The figure shows that a sharp and distinct resonant peak is obtained when D2 equals 1 µm at 1.67 µm wavelength with a loss of 382 dB per cm. As the diameter D3 of a circle increases from 1.55 µm to 1.65 µm, there is a redshift of resonant wavelength from 1.65 µm to 1.66 µm, with peak loss increasing from 223 dB per cm to 263 dB per cm. The highest loss of 346 dB per cm is obtained at D3, equal to 1.75 µm. Typically, enlarging the diameter of the air hole leads to a higher level of confinement loss in PCF. Enlarging the air holes can diminish the efficiency of the photonic bandgap structure in the cladding, resulting in more significant light leakage into the surrounding medium. Increasing the air hole can disrupt the periodicity of the structure. As D3 increases, the core size reduces, affecting the mode properties and overall light guidance within the core. There is often a tradeoff between the air hole diameter and the core size of PCF. After carrying out various numerical simulations using the FEM method, an optimal combination of parameters is found to be D1 equals 1.8 µm, D2 equals 1 µm, and D3 equals 1.65 µm.

6.3.4) Variation of pitch

The figure shows the confinement loss of the proposed sensor dependent on the wavelength with different pitch values. As pitch increases, there is a red shift in resonance wavelength with a loss of 390 dB per centimeter at pitch size 3 micrometer, 263 dB per centimeter at pitch equals 3.3

micrometer, and 428 dB per centimeter at pitch equals 3.4 micrometer. The parameter P controls the distance between the air holes. It directly affects the sensor performance. The magnitude of pitch is chosen to be 3.3 micrometers as it offers lower confinement loss than 3 µm micrometer and 3.4 µm micrometer. CL almost doubles with a 0.1 µm increase in pitch. A favorable channel width is achieved when the pitch is 3.3 micrometers. Thus, the optimum magnitude of pitch is selected to be 3.3 µm micrometers at a resonance wavelength of 1.66 µm micrometer.

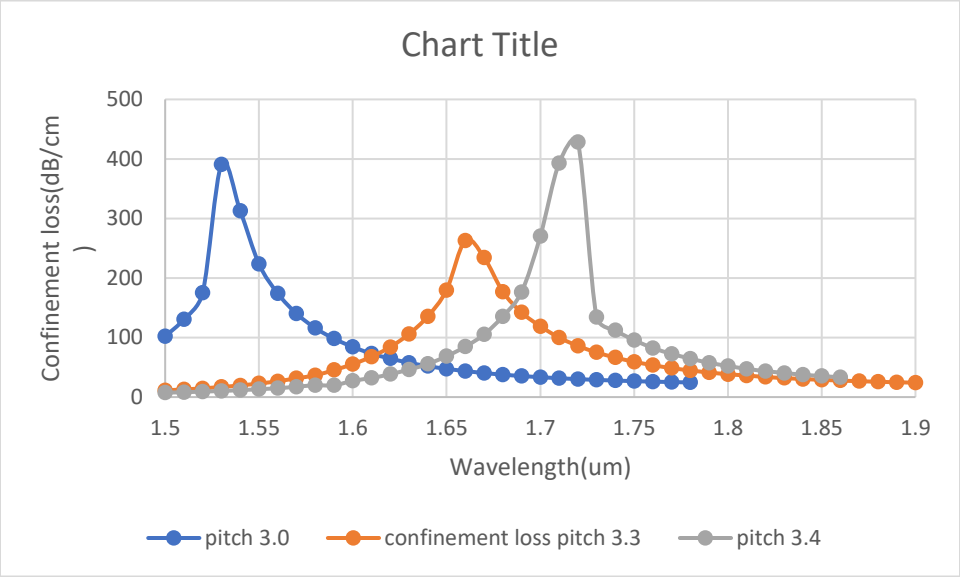

Figure 6.3.4- Loss curves for variation of pitch (distance between air holes)

6.3.5) Variation of the thickness of the Silver layer

Changing the thickness of the silver layer in PCF can substantially influence the plasmonic characteristics and sensing capabilities of the fiber. The main objective of incorporating silver is to modify light's modal characteristics and confinement within the core. The figure shows the sensor's performance characteristics upon changing the silica layer and keeping other parameters constant. A thickness of 65 nm is selected to be the optimized value at resonance wavelength 1.66 µm and confinement loss of 263 dB per cm. A very high peak of 480 dB per cm is achieved at 85 nm thickness. When silica layer thickness increases, damping loss also increases. Variations of silica layer thickness can affect PCF's birefringence and dispersion characteristics. Birefringence refers to the disparity in refractive indices exhibited by the polarized light along

different axes. Moreover, precise control of fabrication techniques, such as the stack and draw method, is necessary to attain the intended thickness.

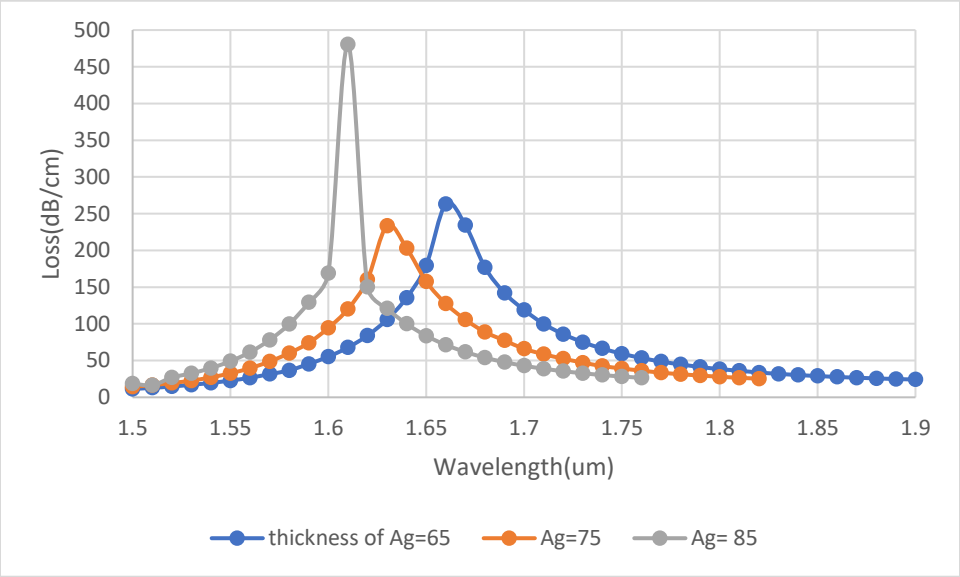

Figure 6.3.5- Loss curves for variation of thickness of silver

6.3.6) Variation of Titanium dioxide layer

The influence of the Titanium dioxide layer on loss spectra is portrayed in the figure. As the depth of TiO2 increases from 5nm to 15nm, a red shift in the resonant wavelength is seen, and rising propagation loss is seen in Figure 6.3.6.

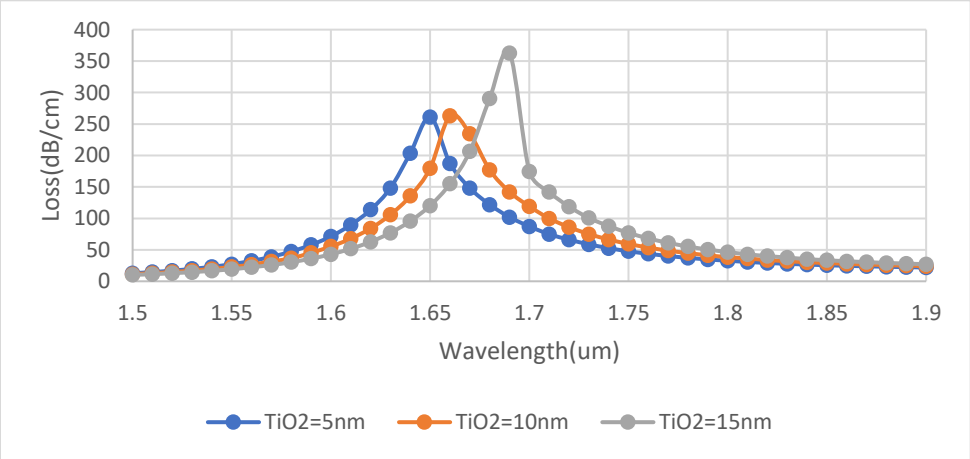

Figure 6.3.6- Loss curves for variation of TiO2 Layer

6.4) Conclusion

By analyzing both the sensors, proposed design 2 has a better wavelength sensitivity of 12000nm/RIU at na=1.37 compared to design 1 with a maximum WS of 7000nm/RIU at na= 1.39. However, design 1 offers a better sensing range than design 2, whose sensing range is 1.36 to 1.39. In design 2, a dual sensing channel is induced by a microchannel and Silica and titanium dioxide configuration, significantly improving the resonance effects. A lower resolution of $8.33\times10-6$ is offered by design 2 compared to design 1 with a resolution of $1.43\times 10-5$. Both designs offer external sensing mechanisms and feasible fabrication techniques.

Chapter 7) Applications and Fabrication

7.1) Introduction

Regular OF have a core consisting of a higher refractive index. Because of the difference in refractive index, light undergoes total internal reflection, propagating through the fiber. Light can propagate through large distances. Traditional fibers have some limitations. Scientists have devised the idea of photonic crystal fiber, which is used to make photonic crystals in the fiber. In the traditional fiber industry, a macroscopic preform exists from where fibers are drawn. The preform is heated in a particular zone. As it gets heated, it becomes soft and is pulled down. Phillip Russel's group took a stack of this preform and heated the stack. When they drew it, a glass structure filled with holes formed. The end structure depends on how the preform is stacked. Therefore, the fiber itself has various holes in the form of whatever is required. Various structures, like dielectric or air core, can be made depending on the stacking method**.**

7.2) Supercontinuum Generation

An essential application of photonic crystal fiber is supercontinuum generation. We require highly monochromatic light, which is a laser for optical experiments. A very short pulse laser is interesting, for example, a 20-femtosecond laser pulse. In nonlinear optics, several interesting experiments can be done if light can be confined in a short laser pulse, resulting in high intensities. One of the popular femtosecond lasers is a Ti Sapphire laser, which can generate femtosecond laser pulses. It becomes problematic to have laser pulses at all wavelengths because Ti Sapphire has a specific gain bandwidth in the region of 800 nanometers. A peak amplitude comes at that point, but it becomes challenging if we want to have output power as a pulse laser at various wavelengths. A broad range of optical radiation at high intensities can be achieved by supercontinuum. In this case, the femtosecond pulse propagates through a photonic crystal fiber, and PCF has solid dispersion because of the complicated bandgap. It converts the incident electromagnetic energy at 800 nm in radiation to a broad range of wavelengths, pulses of high-intensity light. This is called supercontinuum.

To sum up, we can think of photonic crystals as semiconductors of light. The 1D,2D, and 3D modulations of PCF exhibit bandgaps similar to electronic materials.

However, it is an atomic scale in electronic materials, but now it is a much larger scale in nanometers. Just as semiconductors control the propagation of electrical signals, photonic crystals control the propagation of electromagnetic waves. It is a new frontier of photonics. One of the challenges is that it is susceptible to fabrication tolerances. A small amount of disorder can create havoc in observed optical effects. That is one of the difficulties in Photonic Crystal fiber. One key feature is that we should have a strong index contrast to observe these bandgaps. In conventional optical fiber, the difference between the core and cladding indexes is minimal; we want this difference to be as significant as possible in photonic crystals.

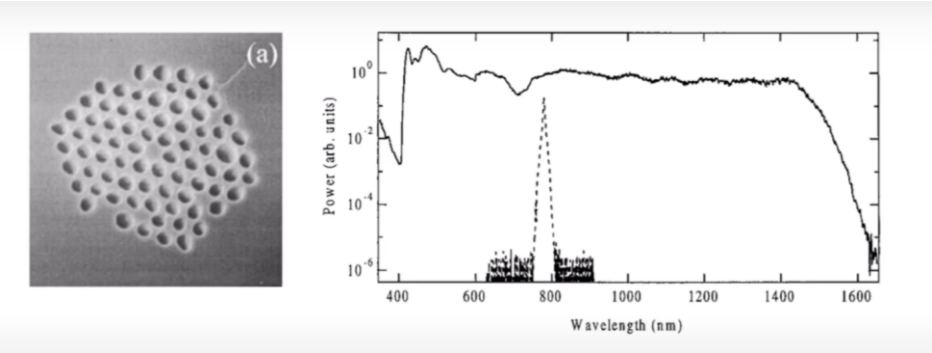

Figure 7.2- Optical spectrum of the continuum generated a 75cm section of microstructure fiber. The dashed curve shows the spectrum of the initial 100 fs pulse [31].

7.3) Fabrication

Three essential methods for the manufacture of PCF are stacking, drawing, and fiber drawing. Millimeters in diameter capillaries are stacked with a solid core in the center. It can take several hours to complete a big stack. Next, the stack is put into a tube and pushed into a fiber drawing furnace. Fiber drawing furnace run at 1900 degrees Celsius. The stack goes into the furnace shortly after, and the glass becomes molten and starts to flow like syrup down to the bottom. A cane comes out ten times smaller than the stack and is typically 2mm in diameter. The cane is collapsed again by another factor of ten by the fiber drawing tower. The cane is pulled out of the furnace and coated in plastic. Finally, it gets rolled up in a drum. By this method, hundreds of meters of structures that are uniform in length can be obtained with an accuracy of a few nanometers. With this extraordinary technology, we can get many nanoscale objects. One unique

aspect of this field is that, unlike other fields where lithography is used to make tiny samples that could take months, we can get hundreds of meters of samples within a day.

7.4) Block diagram and operational mode

Figure 7.4 depicts the experimental configuration and operational principle of the sensor that has been suggested. The setup comprises several components, including a laser for light amplification by stimulated emission of radiation, an optical polarizer, a sensor unit, an optical spectrum analyzer (OSA), a laptop, a programmed pump, an analyte reservoir, and additional elements. An SMF fiber introduces the laser light into the optical polarizer unit. This fiber turns unpolarized light into polarized light and directs it through the sensing unit. The analyte is delivered into the sensing unit through the PVC pipe, and the valve regulates the analyte's flow at a consistent pressure and temperature. The programmable pump sequentially moves the analytes into the sensor unit and then releases them into the waste reservoir. The sensing unit facilitates the interaction between the free electrons of plasmonic material and the photons of the evanescent optical field. The OSA utilizes single-mode fiber (SMF) to receive the polarized light signal from the sensor unit and then measures and quantifies the optical spectra. The laptop collects the measured optical spectra from the Optical Spectrum Analyzer (OSA) using Single-Mode Fiber (SMF) and presents the loss curve of the resonance peak on a monitor. This curve corresponds to each unidentified analyte and is associated with a unique resonance wavelength. The sensor can accurately detect and distinguish various analytes by examining the resonance peak loss curve.

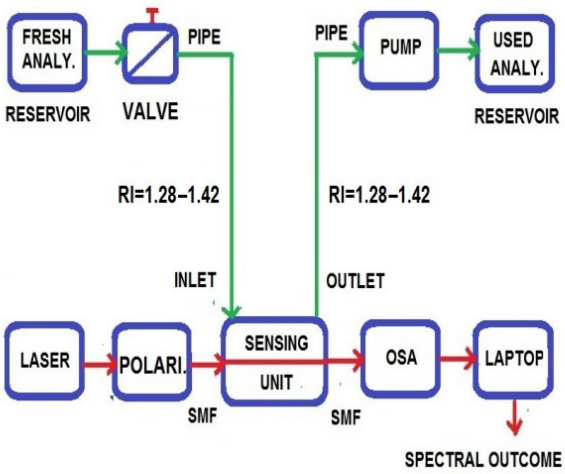

Figure7.4- Experimental configuration of the proposed design.

7.5) Implementing Design 1 for early identification of various cancer cells.

Photonics biosensing platforms possess exceptional advantages in detecting several diseases, including cancer, diabetes, and malaria, because of their high sensitivity, selectivity, and durability. Cancer is an epigenetic condition characterized by the dysregulation of cell division, resulting in the development of tumors within the human body. Timely identification of malignant cells enhances patients' likelihood of survival and improves treatment outcomes. Optical biosensors offer the possibility of rapid and accurate detection, dependable imaging of cancer cells, tracking the development of cancer cells, and assessing the efficiency of anti-cancer chemotherapy drugs. Several techniques, including Raman spectroscopy and surface-enhanced Raman spectroscopy, have been studied to detect cancer cells using PCF-based SPR biosensors.

In this chapter, a dual-core PCF biosensor has been employed for efficient biosensing. This sensor contains two elliptical channels positioned on both sides of the fiber core. PCF possesses desirable characteristics such as flexibility in design, scalability, and efficiency, as well as the ability to control dispersion and exhibit diverse nonlinear properties readily. PCF-SPR imaging solution addresses the limitations of traditional prism-based SPR sensing, including a bulky design, the need for a correct incidence angle, and many adjustable mechanical components. PCF-based biosensors can overcome these constraints. Plasmonic materials play a crucial role in designing and developing sensors in PCF-SPR systems. Here, gold is chosen as the plasmonic

material as it is resistant to oxidation in a wet environment. Consistency in the metal coating is crucial. This sensor is coated with metal on its external surface, making it suitable for manufacture. Using advanced finite element computational techniques, the sensor aims to separate malignant cells from healthy cells accurately. It operates by detecting variations in the resonance peak wavelength caused by differences in the analyte's refractive index.

The proposed biosensor 1 intends to identify different forms of cancer by detecting any refractive index alteration from healthy cells to cancer-affected cells. These cancer types include basal cell carcinoma of the skin, blood cancer cell Jurkat, and breast cancer cell MCF-7. The modal analysis only considers the fundamental Y-polarization mode. The studies are conducted in the XY plane while the incident light wave propagates in the Z-direction. A specific wavelength transformation from the fundamental mode to the plasmon mode results in a significant increase in energy.

Consequently, losses reach maximum values. The proposed design 1 is analyzed for cancer cell detection. The optical sensor that has been demonstrated has the potential to establish an efficient and uncomplicated method for cancer detection, offering low cost and great sensitivity as an alternative to surgical and chemical approaches. The numerical analysis of the sensor has shown promising results with gold coating as a plasmonic material. The amplitude sensitivities are 878/RIU unit for basal and 294.12/RIU unit for MCF-7.

The graphs in the figure display the relationship between wavelength and confinement loss for all cancer types examined in this study. The blue curves represent normal cells, while the orange curve represents cancer-affected cells in the figures. When a regular cell in the analyte channel is replaced by cancerous cells, there is an increase in confinement loss and a shift of the peak towards a longer wavelength. This phenomenon occurs due to the intense contact between the metal and dielectric materials, which is affected by the high value of the analyte refractive index. The primary basis of the amplitude interrogation approach is the displacement of peaks across the wavelength spectrum.

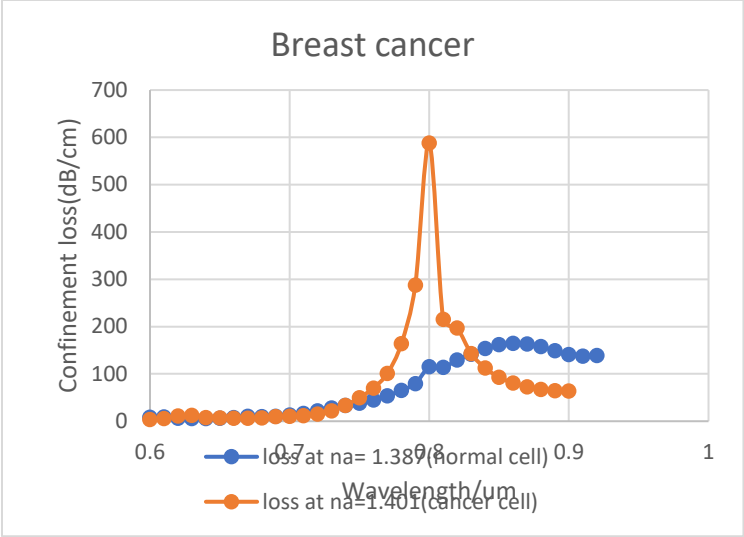

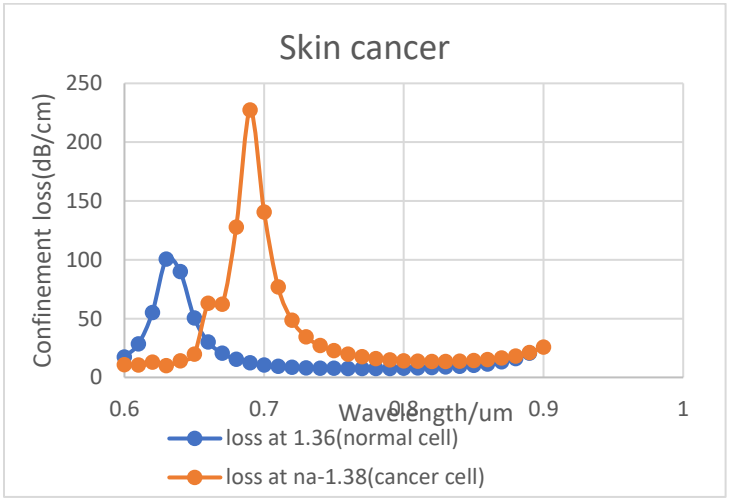

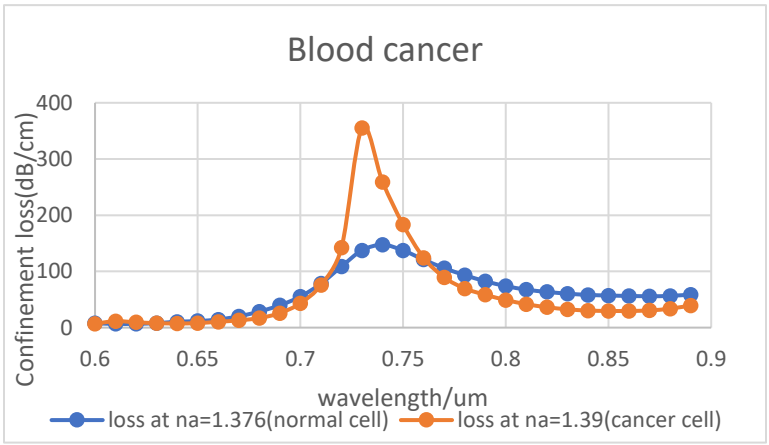

Figure7.5a- The proposed PCF-SPR biosensor exhibits confinement loss features for various normal and cancerous cells.

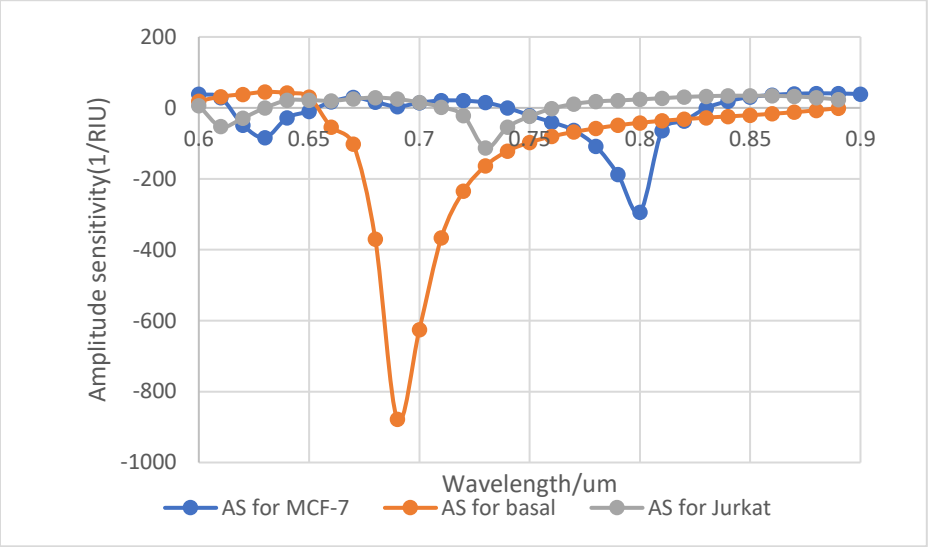

Figure 7.5b The amplitude sensitivities for the detection of cancer-affected cells

Chapter 8) Conclusion

8.1) Socio-economic impact

The PCF SPR biosensor has a substantial influence on the field of medical science and research. Some notable applications are outlined below.

- This type of sensor can be utilized to conduct DNA and RNA assays.
- Deadly viruses such as Dengue can be rapidly identified in gut samples. We can utilize them to analyze antibody-antigen interactions and detect mRNA molecules, hemoglobin levels, hormones, proteins, and more.
- To ascertain the existence of harmful gases such as hydrogen sulfide within a compound mixture, various tests can be finished within 2-10 minutes, resulting in a significant reduction in testing duration.
- In the order of nanograms, only a few molecules are required for the samples, resulting in a lower overall cost.
- The sole options available are the costly commercial instruments, which cost tens of thousands of dollars; therefore, we can achieve significant cost savings by leveraging their use.

8.2) Future Work

In proposed designs 1 and 2, we used circular air holes. Gold and titanium dioxide have been used as plasmonic materials. Silica is used as background material for both designs. In the future, the following improvements can be made in this sector.

- Employ various plasmonic materials such as graphene, indium tin oxide, titanium nitride, aluminum, etc., for enhanced sensitivity and detection limits.
- Elliptical, rectangular, and other types of air holes can be compared to yield superior outcomes.

- Similar designs can be used to do a D-shaped PCF to examine the performance of the sensors.
- The sensing strategies in both designs are external. Attempts to implement an internal sensing strategy for the same design can be made in the future.
- Future research could focus on multiplexed sensing, where various analytes can be detected simultaneously.
- Lab-on-a-chip technologies can result in smaller and more portable sensing platforms. This could be particularly significant for point-of-care diagnostics and on-site environmental monitoring. PCF-based SPR sensors could be developed for biological applications, including real-time monitoring of biomolecular interactions, early illness detection, and medication development.

- Future advancements could enable real-time monitoring of living things, affecting medical diagnosis and research.

8.3) Conclusion

In summary, it can be reliably stated that biosensors play a crucial role in detecting biological and biochemical analytes. This paper used the surface plasmon resonance phenomena to identify the unidentified analyte. The cladding region in PCFs has regularly spaced air holes that guide the electromagnetic field. Consequently, light propagation may be manipulated by altering the geometry of these air holes. Various plasmonic materials are employed to augment the sensitivity of the sensors. The primary factors dictating a sensor's efficiency are the highest amplitude and maximum wavelength sensitivity. We have comprehensively described two distinct SPR biosensor designs, demonstrating exceptional sensing capabilities. The fiber is surrounded by a perfectly matched layer (PML) that ensures the absorption of the scattered evanescent field by both sensors. We employed the complete vectorial finite element technique (FEM) of COMSOL Multiphysics simulation software to conduct numerical investigations. Upon optimizing all the parameters that determine the performance of the fibers, we have obtained exceptional values for amplitude and wavelength sensitivity (AS and WS), confinement loss, and other relevant factors,

as previously discussed.

This paper has suggested and computationally examined two innovative plasmonic refractive index sensors with a double-core structure. These sensors are designed to detect low refractive index values with great sensitivity. Using both microchannel and Ag-TiO2 configuration in the proposed design of sensor 2 resulted in a significant improvement in resonance effects. This led to maximum sensitivities of 12000 nm/RIU and 393 RIU^{-1} using wavelength and amplitude interrogation methods, respectively, within the sensing range of 1.36–1.39. Proposed design one has been tested for detecting various cancer cells, yielding a maximum amplitude sensitivity of $878RIU^{-1}$ for skin cancer cells. Additionally, the inclusion of an external sensing mechanism and practical fabrication processes make the suggested sensors highly suitable for detecting analytes with a lower refractive index, such as drug monitoring and inspection, as well as bio-organic chemicals.

Bibliography

[1] A. M. R. Pinto and M. Lopez-Amo, “Photonic crystal fibers for sensing applications,” *Journal of Sensors*, vol. 2012. 2012. doi: 10.1155/2012/598178.

[2] J. Ortega-Mendoza, A. Padilla-Vivanco, C. Toxqui-Quitl, P. Zaca-Morán, D. Villegas-Hernández, and F. Chávez, “Optical Fiber Sensor Based on Localized Surface Plasmon Resonance Using Silver Nanoparticles Photodeposited on the Optical Fiber End,” *Sensors*, vol. 14, no. 10, pp. 18701–18710, Oct. 2014, doi: 10.3390/s141018701.

[3] A. K. Singh, S. Mittal, M. Das, A. Saharia, and M. Tiwari, “Optical biosensors: a decade in review,” *Alexandria Engineering Journal*, vol. 67, pp. 673–691, Mar. 2023, doi: 10.1016/J.AEJ.2022.12.040.

[4] R. C. Jorgenson and S. S. Yee, “A fiber-optic chemical sensor based on surface plasmon resonance,” *Sens Actuators B Chem*, vol. 12, no. 3, pp. 213–220, Apr. 1993, doi: 10.1016/0925-4005(93)80021-3.

[5] J. N. Dash and R. Jha, “SPR Biosensor Based on Polymer PCF Coated With Conducting Metal Oxide,” *IEEE Photonics Technology Letters*, vol. 26, no. 6, pp. 595–598, Mar. 2014, doi: 10.1109/LPT.2014.2301153.

[6] J. N. Dash and R. Jha, “On the Performance of Graphene-Based D-Shaped Photonic Crystal Fibre Biosensor Using Surface Plasmon Resonance,” *Plasmonics*, vol. 10, no. 5, pp. 1123–1131, Oct. 2015, doi: 10.1007/S11468-015-9912-7/METRICS.

[7] S. Jiao, S. Gu, H. Fang, and H. Yang, “Analysis of Dual-Core Photonic Crystal Fiber Based on Surface Plasmon Resonance Sensor with Segmented Silver Film,” *Plasmonics*, vol. 14, no. 3, pp. 685–693, Jun. 2019, doi: 10.1007/S11468-018-0846-8/METRICS.

[8] B. Liu, Y. Lu, X. Yang, and J. Yao, “Tunable Surface Plasmon Resonance Sensor Based on Photonic Crystal Fiber Filled with Gold Nanoshells,” *Plasmonics*, vol. 13, no. 3, pp. 763–770, Jun. 2018, doi: 10.1007/S11468-017-0570-9.

[9] M. R. Hasan, S. Akter, A. A. Rifat, S. Rana, and S. Ali, “A Highly Sensitive Gold-Coated Photonic Crystal Fiber Biosensor Based on Surface Plasmon Resonance,” *Photonics 2017, Vol. 4, Page 18*, vol. 4, no. 1, p. 18, Mar. 2017, doi: 10.3390/PHOTONICS4010018.

[10] K. Labeeb and S. K. Biswas, “Numerical Investigation of Ultra-high Negative Dispersion Compensating Octagonal Photonic Crystal Fiber with High Nonlinearity,” *2019 10th International Conference on Computing, Communication and Networking Technologies, ICCCNT 2019*, Jul. 2019, doi: 10.1109/ICCCNT45670.2019.8944543.

[11] M. N. Hossen, M. Ferdous, M. Abdul Khalek, S. Chakma, B. K. Paul, and K. Ahmed, “Design and analysis of biosensor based on surface plasmon resonance,” *Sens Biosensing Res*, vol. 21, pp. 1–6, Nov. 2018, doi: 10.1016/J.SBSR.2018.08.003.

[12] M. Rakibul Islam, M. M. I. Khan, F. Mehjabin, J. Alam Chowdhury, and M. Islam, “Design of a fabrication friendly & highly sensitive surface plasmon resonance-based photonic crystal fiber biosensor,” *Results Phys*, vol. 19, p. 103501, Dec. 2020, doi: 10.1016/J.RINP.2020.103501.

[13] W. Gao *et al.*, “Experimental investigation on supercontinuum generation by single, dual, and triple wavelength pumping in a silica photonic crystal fiber,” *Appl Opt*, vol. 55, no. 33, p. 9514, Nov. 2016, doi: 10.1364/ao.55.009514.

[14] A. Aming, M. Uthman, R. Chitaree, W. Mohammed, and B. M. A. Rahman, “Design and Characterization of Porous Core Polarization Maintaining Photonic Crystal Fiber for THz Guidance,” *Journal of Lightwave Technology*, vol. 34, no. 23, pp. 5583–5590, Dec. 2016, doi: 10.1109/JLT.2016.2623657.

[15] N. Muduli and H. K. Padhy, “An optimized configuration of large mode field area PMMA photonic crystal fiber with low bending loss: a new approach,” *Journal of materials science. Materials in electronics*, no. 2, pp. 1906–1912, Feb. 2016, Accessed: Nov. 12, 2023. [Online]. Available: https://dal.novanet.ca

[16] K. Nielsen, O. Bang, P. U. Jepsen, A. J. L. Adam, P. C. M. Planken, and H. K. Rasmussen, "Bendable, low-loss Topas fibers for the terahertz frequency range," *Optics Express, Vol. 17, Issue 10, pp. 8592-8601*, vol. 17, no. 10, pp. 8592–8601, May 2009, doi: 10.1364/OE.17.008592.

[17] K. Nielsen, O. Bang, H. Bao, P. U. Jepsen, and H. K. Rasmussen, "Fabrication and characterization of porous-core honeycomb bandgap THz fibers," *Optics Express, Vol. 20, Issue 28, pp. 29507-29517*, vol. 20, no. 28, pp. 29507–29517, Dec. 2012, doi: 10.1364/OE.20.029507.

[18] H. Han, H. Park, M. Cho, and J. Kim, "Terahertz pulse propagation in a plastic photonic crystal fiber," *Appl Phys Lett*, vol. 80, no. 15, pp. 2634–2636, Apr. 2002, doi: 10.1063/1.1468897.

[19] Md. R. Hasan, S. M. A. Razzak, Md. A. Islam, and M. S. Anower, "Low-loss and bend-insensitive terahertz fiber using a rhombic-shaped core," *Applied Optics, Vol. 55, Issue 30, pp. 8441-8447*, vol. 55, no. 30, pp. 8441–8447, Oct. 2016, doi: 10.1364/AO.55.008441.

[20] J. Noda, K. Okamoto, and Y. Sasaki, "Polarization-Maintaining Fibers and Their Applications," *Journal of Lightwave Technology*, vol. 4, no. 8, pp. 1071–1089, 1986, doi: 10.1109/JLT.1986.1074847.

[21] N. A. Mortensen, J. Lægsgaard, and A. Bjarklev, "Mode areas and field-energy distribution in honeycomb photonic bandgap fibers," *JOSA B, Vol. 20, Issue 10, pp. 2037-2045*, vol. 20, no. 10, pp. 2037–2045, Oct. 2003, doi: 10.1364/JOSAB.20.002037.

[22] N. A. Mortensen, J. Lægsgaard, and A. Bjarklev, "Mode areas and field-energy distribution in honeycomb photonic bandgap fibers," *JOSA B, Vol. 20, Issue 10, pp. 2037-2045*, vol. 20, no. 10, pp. 2037–2045, Oct. 2003, doi: 10.1364/JOSAB.20.002037.

[23] P. S. Maji and P. R. Chaudhuri, "Geometrical parameters dependence towards ultra-flat dispersion square-lattice PCF using tunable liquid infiltration," *WRAP 2013 - Workshop on Recent Advances in Photonics*, Oct. 2014, doi: 10.1109/WRAP.2013.6917653.

[24] R. Islam, M. S. Habib, G. K. M. Hasanuzzaman, S. Rana, M. A. Sadath, and C. Markos, “A Novel Low-Loss Diamond-Core Porous Fiber for Polarization Maintaining Terahertz Transmission,” *IEEE Photonics Technology Letters*, vol. 28, no. 14, pp. 1537–1540, Jul. 2016, doi: 10.1109/LPT.2016.2550205.

[25] K. Ahmed and M. Morshed, “Design and numerical analysis of microstructured-core octagonal photonic crystal fiber for sensing applications,” *Sens Biosensing Res*, vol. 7, pp. 1–6, Mar. 2016, doi: 10.1016/J.SBSR.2015.10.005.

[26] S. Li, “Equiangular spiral photonic crystal fiber for code synchronization in all-optical analog-to-digital conversion based on lumped time delay compensation scheme,” *Optik (Stuttg)*, vol. 127, no. 11, pp. 4693–4697, Jun. 2016, doi: 10.1016/J.IJLEO.2016.02.017.

[27] S. Luke, S. K. Sudheer, and V. P. M. Pillai, “Tellurite based circular photonic crystal fiber with high nonlinearity and low confinement loss,” *Optik (Stuttg)*, vol. 127, no. 23, pp. 11138–11142, Dec. 2016, doi: 10.1016/J.IJLEO.2016.09.024.

[28] A. Cerqueira S., Jr., C. M. B. Cordeiro, F. Biancalana, P. J. Roberts, H. E. Hernandez-Figueroa, and C. H. B. Cruz, “Nonlinear interaction between two different photonic bandgaps of a hybrid photonic crystal fiber,” *Optics Letters, Vol. 33, Issue 18, pp. 2080-2082*, vol. 33, no. 18, pp. 2080–2082, Sep. 2008, doi: 10.1364/OL.33.002080.

[29] T.-F. Kao, C.-K. Sun, H.-W. Chen, L.-J. Chen, and J.-Y. Lu, “Low-loss subwavelength plastic fiber for terahertz waveguiding,” *Optics Letters, Vol. 31, Issue 3, pp. 308-310*, vol. 31, no. 3, pp. 308–310, Feb. 2006, doi: 10.1364/OL.31.000308.

[30] T. A. Roni, R. Hassan, and M. Faisal, “Dual-side polished SPR biosensor with wide sensing range,” in *Proceedings of 2020 11th International Conference on Electrical and Computer Engineering, ICECE 2020*, Institute of Electrical and Electronics Engineers Inc., Dec. 2020, pp. 487–490. doi: 10.1109/ICECE51571.2020.9393102.

[31] “(122) 5.5 Applications of Photonic Crystals - YouTube.” Accessed: Dec. 19, 2023. [Online]. Available: https://www.youtube.com/watch?v=LMsKP1ui9fI&t=627s

[32] L. Han and L. Han, “1D Photonic Crystals: Principles and Applications in Silicon Photonics,” *Theoretical Foundations and Application of Photonic Crystals*, Dec. 2017, doi: 10.5772/INTECHOPEN.71753.

[33] A. M. R. Pinto and M. Lopez-Amo, “Photonic Crystal Fibers for Sensing Applications,” *J Sens*, vol. 2012, pp. 1–21, 2012, doi: 10.1155/2012/598178.

[34] D. J. J. Hu, Z. Xu, and P. P. Shum, “Review on Photonic Crystal Fibers with Hybrid Guiding Mechanisms,” *IEEE Access*, vol. 7, pp. 67469–67482, 2019, doi: 10.1109/ACCESS.2019.2917892.

[35] M. S. Islam *et al.*, “A V-shaped ultra-sensitive Localized Surface Plasmon Resonance based Biochemical sensor,” *IEEE Access*, vol. 7, pp. 79085–79094, Mar. 2021, doi: 10.1109/ACCESS.2019.2922663.

[36] R. Bakhtiar, “Surface plasmon resonance spectroscopy: A versatile technique in a biochemist’s toolbox,” *J Chem Educ*, vol. 90, no. 2, pp. 203–209, Feb. 2013, doi: 10.1021/ED200549G.

[37] “XanTec bioanalytics GmbH | Tech notes | Optics.” Accessed: Nov. 27, 2023. [Online]. Available: https://www.xantec.com/technotes/optics.php

[38] “(62) An overview of surface plasmon resonance (SPR) - YouTube.” Accessed: Nov. 27, 2023. [Online]. Available: https://www.youtube.com/watch?v=4eet-rjAHic&t=19s

[39] B. Gauvreau, A. Hassani, M. Fassi Fehri, A. Kabashin, and M. A. Skorobogatiy, “Photonic bandgap fiber-based Surface Plasmon Resonance sensors,” *Opt Express*, vol. 15, no. 18, p. 11413, 2007, doi: 10.1364/OE.15.011413.

[40] S. Unser, I. Bruzas, J. He, and L. Sagle, “Localized Surface Plasmon Resonance Biosensing: Current Challenges and Approaches,” *Sensors 2015, Vol. 15, Pages 15684-15716*, vol. 15, no. 7, pp. 15684–15716, Jul. 2015, doi: 10.3390/S150715684.

[41] M. Piliarik *et al.*, “Surface plasmon resonance (SPR) sensors: approaching their limits?” *Optics Express, Vol. 17, Issue 19, pp. 16505-16517*, vol. 17, no. 19, pp. 16505–16517, Sep. 2009, doi: 10.1364/OE.17.016505.

[42] R. S. Abraham, D. R. Barnidge, and I. R. Lanza, “Assessment of proteins of the immune system,” *Clinical Immunology: Principles and Practice: Fourth Edition*, pp. 1145–1159, 2013, doi: 10.1016/B978-0-7234-3691-1.00106-9.

[43] I. Danlard and E. K. Akowuah, “Assaying with PCF-based SPR refractive index biosensors: From recent configurations to outstanding detection limits,” *Optical Fiber Technology*, vol. 54, p. 102083, Jan. 2020, doi: 10.1016/J.YOFTE.2019.102083.

[44] M. Hautakorpi, M. Mattinen, and H. Ludvigsen, “Surface-plasmon-resonance sensor based on three-hole microstructured optical fiber,” *Opt Express*, vol. 16, no. 12, p. 8427, Jun. 2008, doi: 10.1364/OE.16.008427.

[45] N. Luan, R. Wang, W. Lv, and J. Yao, “Surface plasmon resonance sensor based on D-shaped microstructured optical fiber with a hollow core,” *Opt Express*, vol. 23, no. 7, p. 8576, Apr. 2015, doi: 10.1364/OE.23.008576.

[46] N. Luan and J. Yao, “Refractive Index and Temperature Sensing Based on Surface Plasmon Resonance and Directional Resonance Coupling in a PCF,” *IEEE Photonics J*, vol. 9, no. 2, pp. 1–7, Apr. 2017, doi: 10.1109/JPHOT.2017.2667878.

[47] T. Ahmed, A. K. Paul, Md. S. Anower, and S. M. A. Razzak, “Surface plasmon resonance biosensor based on hexagonal lattice dual-core photonic crystal fiber,” *Appl Opt*, vol. 58, no. 31, p. 8416, Nov. 2019, doi: 10.1364/AO.58.008416.

[48] C. Caucheteur, T. Guo, and J. Albert, “Review of plasmonic fiber optic biochemical sensors: improving the limit of detection,” *Anal Bioanal Chem*, vol. 407, no. 14, pp. 3883–3897, May 2015, doi: 10.1007/s00216-014-8411-6.

[49] A. Rifat, G. Mahdiraji, D. Chow, Y. Shee, R. Ahmed, and F. Adikan, “Photonic Crystal Fiber-Based Surface Plasmon Resonance Sensor with Selective Analyte Channels and Graphene-Silver Deposited Core,” *Sensors*, vol. 15, no. 5, pp. 11499–11510, May 2015, doi: 10.3390/s150511499.

[50] E. K. Akowuah, T. Gorman, H. Ademgil, and S. Haxha, “A highly sensitive photonic crystal fiber (PCF) surface plasmon resonance (SPR) sensor based on a bimetallic structure of gold and silver,” in *2012 IEEE 4th International Conference on Adaptive Science & Technology (ICAST)*, IEEE, Oct. 2012, pp. 121–125. doi: 10.1109/ICASTech.2012.6381078.

[51] A. H. El-Saeed, A. E. Khalil, M. F. O. Hameed, M. Y. Azab, and S. S. A. Obayya, “Highly sensitive SPR PCF biosensors based on Ag/TiN and Ag/ZrN configurations,” *Opt Quantum Electron*, vol. 51, no. 2, p. 56, Feb. 2019, doi: 10.1007/s11082-019-1764-5.

[52] Md. S. Islam *et al.*, “A Hi-Bi Ultra-Sensitive Surface Plasmon Resonance Fiber Sensor,” *IEEE Access*, vol. 7, pp. 79085–79094, 2019, doi: 10.1109/ACCESS.2019.2922663.

[53] B. Lee, S. Roh, and J. Park, “Current status of micro- and nano-structured optical fiber sensors,” *Optical Fiber Technology*, vol. 15, no. 3, pp. 209–221, 2009, doi: 10.1016/J.YOFTE.2009.02.006.

[54] Q. Liu *et al.*, “Mid-infrared surface plasmon resonance sensor based on photonic crystal fibers,” *Optics Express, Vol. 25, Issue 13, pp. 14227-14237*, vol. 25, no. 13, pp. 14227–14237, Jun. 2017, doi: 10.1364/OE.25.014227.

[55] R. Otupiri, E. K. Akowuah, and S. Haxha, “Multi-channel SPR biosensor based on PCF for multi-analyte sensing applications,” *Opt Express*, vol. 23, no. 12, p. 15716, Jun. 2015, doi: 10.1364/OE.23.015716.

[56] A. K. Paul, M. A. Mollah, M. Z. Hassan, N. Gomez-Cardona, and E. Reyes-Vera, “Graphene-Coated Highly Sensitive Photonic Crystal Fiber Surface Plasmon Resonance Sensor for Aqueous Solution: Design and Numerical Analysis,” *Photonics 2021, Vol. 8, Page 155*, vol. 8, no. 5, p. 155, May 2021, doi: 10.3390/PHOTONICS8050155.

[57] H. N. Rafi and J. Islam, “Air-hole attributed performance of photonic crystal fiber-based SPR sensors,” 2020, doi: 10.1016/j.sbsr.2020.100364.

[58] M. Sun, “Nanoparticle Catalysis by Surface Plasmon,” *New and Future Developments in Catalysis: Catalysis by Nanoparticles*, pp. 473–487, 2013, doi: 10.1016/B978-0-444-53874-1.00021-4.